Third-Order Elastic Constants of Calcite*

H. KAGA†

Department of Metallurgy and Materials Research Laboratory, Universty of Illinois, Urbana, Illinois

(Received 11 March 1968)

The third-order elastic constants of calcite at 0°C have been determined by measuring the stress and temperature dependence of sound velocities in it by means of an improved pulse-superposition method (average sensitivity of 2×10^{-7}). Within the small temperature range considered (about 2°C), a nonlinear temperature dependence which varies with pressure has been clearly observed. Out of 14 independent third-order moduli, C_{114} and C_{134} are definitely positive, and all the others are negative, with ambiguities for C_{124} and C_{444}. The approximate magnitude is equally large for C_{111}, C_{222}, and C_{333}, intermediate for C_{112}, C_{113}, C_{114}, C_{133}, C_{155}, C_{344}, and very small for C_{123}, C_{124}, C_{134}, C_{144}, C_{444}. The pressure derivative of the bulk modulus calculated using these constants is in reasonable agreement with Bridgman's data for the change in compressibility with pressure. The contribution of the ion-core, short-range repulsive interaction $C_{ijk}{}^R$ to the third-order elastic constants has been evaluated for the carbonate and nitrate crystals of the calcite type using an inverse-power potential. The repulsive contributions were found to be predominant over the other contributions to almost all the third-order constants. Under the assumption that the remaining contribution is the electrostatic interaction alone, and using the experimental data for calcite, complete sets of the third-order constants have been estimated for other carbonate crystals.

I. INTRODUCTION

ELASTIC constants can provide insight into the nature of the binding forces between atoms in a crystal because they are represented through the derivatives of the interatomic potentials. In the Born-model evaluation of the cohesive energy of an ionic crystal, the bulk modulus assesses the relative importance of the long-range Coulombic and the short-range repulsive interactions for the total cohesive energy as well as the parameters of the ion-core repulsive potential.[1] The Cauchy relations for the elastic constants test for the existence of many-body forces in addition to the simple two-body interactions.[2,3] The analysis of the deviations from Cauchy relations by means of a detailed quantum-mechanical calculation of the elastic constants should give us information about these many-body forces, that is, whether they are primarily ion-overlap interactions, covalent interactions, or an admixture of these.[4–6] One can also examine individual terms in the total interatomic potential by systematically measuring the elastic constants while changing such parameters as valence electron density (electron-atom ratio), ion-core charge, lattice constant, crystal structure, and so forth.

Third-order elastic constants are of special interest because they are related to all anharmonic properties of solids as the coefficients of the first-order anharmonic terms in the interatomic potential. Thus they determine anharmonic properties such as thermal expansion, temperature, and stress dependence of elastic constants, behavior of the heat capacity above the Debye temperature, and phonon-phonon interactions. Thermal expansion produces the difference between adiabatic and isothermal elastic constants. The interaction between acoustic and lattice phonons explains one of the mechanisms of ultrasonic attenuation in solids, which is expressed in terms of third-order elastic constants through the generalized Grüneisen mode parameters.[7] Third-order elastic constants are also indispensable for finite elasticity theory,[8] where the elastic stress is nonlinear with the elastic strain, and therefore, in certain crystallographic planes in a crystal, the elastic shear behavior is asymmetric with respect to the sense of the shear displacement. Although the anharmonic deviations from the harmonic properties are, in general, small in magnitude, they are all qualitatively important phenomena that cannot be understood in the framework of the harmonic approximation. Furthermore, third-order elastic constants can furnish knowledge about the ion-core repulsive interactions and other potentials which vary rapidly with the interionic separation, because these contributions usually become predominant in the higher derivatives.

In recent years considerable attention has been given both to the theoretical and experimental determination of third-order elastic constants in solids. During this time several ingenious experimental methods of high sensitivity have been developed, which permit the resolution of very small ultrasonic velocity changes. In the same period theoretical computations of third-order elastic constants were first carried out for alkali-halide ionic crystals, because their cohesive energies can be relevantly expressed in terms of the Born-model ap-

* Supported in part by the U. S. Atomic Energy Commission under Contract No. AT(11-1)-1198, and also by the U. S. Army Research Office (Durham).

† On leave of absence from Central Research Laboratory, Fuji Iron and Steel Co., Ltd., Sagamihara, Kanagawa, Japan.

[1] M. P. Tosi, Solid State Phys. **16**, 1 (1964).

[2] P. O. Löwdin, Advan. Phys. **5**, 1 (1956).

[3] T. Kurosawa, in *Bussie Kouza*, edited by K. Ariyama *et al.* (Kyoritsu Publication Inc., Tokyo, 1959), Vol. XI, p. 151.

[4] P. O. Löwdin, Ph.D. thesis, Uppsala, 1948 (unpublished).

[5] P. O. Löwdin, J. Chem. Phys. **18**, 365 (1950).

[6] J. Yamashita and T. Kurosawa, J. Phys. Soc. Japan **9**, 944 (1954).

[7] W. P. Mason, in *Physical Acoustics*, edited by W. P. Mason (Academic Press Inc., New York, 1965), Vol. IIIB, p. 235.

[8] F. D. Murnaghan, *Finite Deformation of an Elastic Solid* (John Wiley & Sons, Inc., New York, 1951).

proximation.[9–12] Then it was extended to diamond-like crystals (Ge, Si) in which the six third-order elastic constants were evaluated in terms of three force constants fitted to match experimental values.[13] The third-order constants of fluorite crystals (CaF_2, SrF_2, BaF_2) have also been calculated on the basis of rigid-ion and dipole shell models.[14] Calculations have been attempted for metallic crystals such as the alkalis,[15] noble,[16] and other cubic ones[17,18] using a simple potential consisting of the electrostatic attractive and repulsive, and Fermi energy terms,[15,16,18] or the model Morse potential.[17]

Experimental measurements of complete set of a third-order elastic constants have now covered the following materials: semiconductors (Ge,[19–22] Si,[20,21] GaAs,[23] phosphorus-doped n-type Si[24]); ionic crystals (NaCl,[25,26] KCl,[25] MgO,[22] BaF_2[27]); metals (Cu,[28,29] Ag,[28] Au[28], β-brass,[26] Al[18]); trigonal α-quartz[30]; and several polycrystalline solids (Pyrex glass,[31] polystyrene,[31] iron,[31] steel,[32] Al alloy,[32] Mg,[32] Mo,[32] W,[32] and fused SiO_2 [22]). The experimental methods used were: McSkimin's pulse-superposition method[33] in Refs. 19, 21, 22, 23, 27, and 30; the sing-around method developed by Forgacs[34] in Refs. 20 and 29; the two-specimen interference method[28] in Refs. 18, 26, and 28; the two-echo cancellation method[35,36] in Ref. 25; the pulsed-oscillator continuous-wave (cw)-echo cancellation method in Ref. 32; and Blume's phase-quadrature method[37] in Ref. 24.

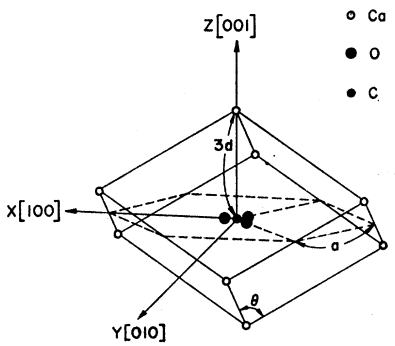

FIG. 1. A cleavage rhombohedral pseudocell of calcite. For clarity atoms are shown only at the corners and the center of this cell; not shown are Ca atoms situated at the centers of the 6 faces and CO_3 groups at the centers of 12 edges.

There are also a large number of measurements of the hydrostatic pressure dependence of second-order elastic constants. These have served to check certain linear combinations of newly determined third-order constants, and to provide nondirectional information about anharmonic forces.

At the present time, α-quartz is the only noncubic crystal for which a full set of third-order constants is available. When one passes to a crystal with lower symmetry, the greater number of elastic constants requires a greater number of experimental measurements to determine the complete set. Thus experimental error is more likely. Calcite is a trigonal crystal, typical of the homologous series of carbonates, and is well known for its optical birefringence. Calcite, whose structure is given in Fig. 1, has unusual thermal-expansion coefficients at room temperature. The linear-expansion coefficient is large and positive in the direction of the threefold Z axis, and is small and negative in the directions perpendicular to it (Table II B). Another characteristic property of calcite crystal is that deformation twins form in it easily.[38] This might be reflected in a marked difference in the nonlinear elastic behavior for shears in the twinning direction and shears in the antitwinning direction. This nonlinearity may be determined by the effective shear modulus, which is a linear combination of the third-order elastic constants, given as a function of either the shear stress or the shear strain by finite elasticity theory.[8] Furthermore, the nature of the bonding between calcium ions and CO_3 radicals is not yet clarified, although it is known that within CO_3 radicals each carbon atom forms covalent bonds with the surrounding three oxygen atoms by trigonal-planar electron-pair bonds.[39] Therefore, it has been of considerable interest to measure the third-order

[9] H. Bross, Z. Physik **175**, 345 (1963).
[10] A. A. Nranyan, Fiz. Tverd. Tela **5**, 177 (1963); **5**, 1865 (1963) [English transl.: Soviet Phys.—Solid State **5**, 129 (1963); **5**, 1361 (1964)].
[11] P. B. Ghate, Phys. Rev. **139**, A1666 (1965).
[12] R. C. Lincoln, K. M. Koliwad, and P. B. Ghate, Phys. Status Solidi **18**, 265 (1966).
[13] P. N. Keating, Phys. Rev. **149**, 674 (1966).
[14] R. Srinivasan, Bull. Am. Phys. Soc. **12**, 305 (1967).
[15] T. Suzuki and A. V. Granato, Bull. Am. Phys. Soc. **12**, 305 (1967).
[16] C. S. G. Cousins, Proc. Phys. Soc. (London) **91**, 235 (1967).
[17] R. C. Lincoln, K. M. Koliwad, and P. B. Ghate, Phys. Rev. **157**, 463 (1967).
[18] J. F. Thomas, Jr., Ph.D. thesis, University of Illinois, Urbana, Illinois, 1968 (unpublished); and private communication.
[19] T. Bateman, W. P. Mason, and H. J. McSkimin, J. Appl. Phys. **32**, 928 (1961).
[20] J. R. Drabble and M. Gluyas, in *Lattice Dynamics*, edited by R. F. Wallis (Pergamon Press, Inc., New York, 1965), p. 603.
[21] H. J. McSkimin and P. Andreatch, Jr., J. Appl. Phys. **35**, 3312 (1964).
[22] E. H. Bogardus, J. Appl. Phys. **36**, 2504 (1965).
[23] H. J. McSkimin and P. Andreatch, Jr., J. Appl. Phys. **38**, 2610 (1967).
[24] J. J. Hall, Phys. Rev. **161**, 756 (1967).
[25] Z. P. Chang, Phys. Rev. **140**, A1788 (1965).
[26] K. D. Swartz, J. Acoust. Soc. Am. **41**, 1083 (1967); K. D. Swartz, Ph.D. thesis, University of Illinois, Urbana, Illinois, 1966 (unpublished); and private communication.
[27] D. Gerlich, Phys. Rev. **168**, 947 (1968).
[28] Y. Hiki and A. V. Granato, Phys. Rev. **144**, 411 (1966).
[29] K. Salama and G. A. Alers, Phys. Rev. **161**, 673 (1967).
[30] R. N. Thurston, H. J. McSkimin, and P. Andreatch, Jr., J. Appl. Phys. **37**, 267 (1966).
[31] D. S. Hughes and J. L. Kelly, Phys. Rev. **92**, 1145 (1953).
[32] R. T. Smith, R. Stern, and R. W. B. Stephens, J. Acoust. Soc. Am. **40**, 1002 (1966).
[33] H. J. McSkimin, J. Acoust. Soc. Am. **37**, 864 (1965).
[34] R. L. Forgacs, IEEE Trans. Instr. Methods **9**, 359 (1960).
[35] J. Williams and J. Lamb, J. Acoust. Soc. Am. **30**, 308 (1958).
[36] A. D. Colvin, Master's thesis, Rensselaer Polytechnic Institute, Troy, N. Y., 1959 (unpublished).
[37] R. J. Blume, Rev. Sci. Instr. **34**, 1400 (1963).
[38] F. J. Turner, D. T. Griggs, and H. Heard, Bull. Geol. Soc. Am. **65**, 883 (1954).
[39] H. B. Gray, *Electrons and Chemical Bonding* (W. A. Benjamin, Inc., New York, 1965), p. 117.

elastic constants in calcite and to investigate relationships between its properties and its elastic anharmonicity.

II. THEORETICAL FOUNDATION

A. Expressions for Elastic Constants

We use Brugger's definition of elastic constants.[40] In any order, they can be defined as the coefficients of the terms in the elastic strain-energy density expanded into a power series of Lagrangian strain components η_{ij}. The Lagrangian strain components η_{ij}'s are expressed as

$$\eta_{ij}=\frac{1}{2}\left(\frac{\partial x_k}{\partial a_i}\frac{\partial x_k}{\partial a_j}-\delta_{ij}\right), \quad i, j, k=1, 2, 3, \tag{1}$$

where a_i and x_k are the components of the Cartesian coordinates of a material in the undeformed and deformed states, respectively. Summation over all repeated indices is hereafter implied.

In the case of a trigonal crystal, the elastic-strain energy density $\Delta\Phi$ at 0°K is explicitly written up to terms cubic in Lagrangian strains as follows:

$$\begin{aligned}\Delta\Phi(\eta)=\Phi(\eta)-\Phi(0)=\Phi_2+\Phi_3+\cdots=&\tfrac{1}{2}c_{11}(\eta_{11}^2+\eta_{22}^2)+c_{12}\eta_{11}\eta_{22}\\
&+c_{13}(\eta_{22}\eta_{33}+\eta_{33}\eta_{11})+c_{14}\{(\eta_{11}-\eta_{22})(\eta_{23}+\eta_{32})+(\eta_{31}+\eta_{13})(\eta_{12}+\eta_{21})\}+\tfrac{1}{2}c_{33}\eta_{33}^2\\
&+c_{44}(\eta_{23}^2+\eta_{32}^2+\eta_{31}^2+\eta_{13}^2)+\tfrac{1}{2}(c_{11}-c_{12})(\eta_{12}^2+\eta_{21}^2)+\tfrac{1}{6}C_{111}\eta_{11}^3+\tfrac{1}{2}C_{112}\eta_{11}^2\eta_{22}+\tfrac{1}{2}C_{113}(\eta_{11}^2\eta_{33}+\eta_{22}^2\eta_{11})\\
&+\tfrac{1}{2}C_{114}\eta_{11}^2(\eta_{23}+\eta_{32})+C_{123}\eta_{11}\eta_{22}\eta_{33}+C_{124}\{\eta_{11}\eta_{22}(\eta_{23}+\eta_{32})+(\eta_{23}+\eta_{32})(\eta_{12}^2+\eta_{21}^2)\}\\
&+\tfrac{1}{2}C_{133}\eta_{33}^2(\eta_{11}+\eta_{22})+C_{134}\eta_{33}\{(\eta_{11}-\eta_{22})(\eta_{23}+\eta_{32})+(\eta_{31}+\eta_{13})(\eta_{12}+\eta_{21})\}+C_{144}\{\eta_{23}^2+\eta_{32}^2)\\
&+\eta_{22}(\eta_{31}^2+\eta_{13}^2)\}+C_{155}\{\eta_{22}(\eta_{23}^2+\eta_{32}^2)+\eta_{11}(\eta_{31}^2+\eta_{13}^2)\}+\tfrac{1}{6}C_{222}\eta_{22}^3+\tfrac{1}{6}C_{333}\eta_{33}^3+C_{344}\eta_{33}\{(\eta_{23}^2+\eta_{32}^2)\\
&+(\eta_{31}^2+\eta_{13}^2)\}+C_{444}\{\tfrac{1}{6}(\eta_{23}+\eta_{32})^3-(\eta_{23}+\eta_{32})(\eta_{31}^2+\eta_{13}^2)\}+\tfrac{1}{2}(C_{111}+C_{112}-C_{222})\eta_{22}^2\eta_{11}\\
&+\tfrac{1}{2}(-C_{114}-2C_{124})\eta_{22}^2(\eta_{23}+\eta_{32})+\tfrac{1}{4}(-2C_{111}-C_{112}+3C_{222})\eta_{11}(\eta_{12}^2+\eta_{21}^2)+\tfrac{1}{4}(2C_{111}-C_{112}-C_{222})\\
&\times\eta_{22}(\eta_{12}^2+\eta_{21}^2)+\tfrac{1}{2}(C_{113}-C_{123})\eta_{33}(\eta_{12}^2+\eta_{21}^2)+\tfrac{1}{2}(C_{114}+3C_{124})\eta_{11}(\eta_{31}+\eta_{13})(\eta_{12}+\eta_{21})\\
&+\tfrac{1}{2}(C_{114}-C_{124})\eta_{22}(\eta_{31}+\eta_{13})(\eta_{12}+\eta_{21})+\tfrac{1}{2}(-C_{144}+C_{155})(\eta_{23}+\eta_{32})(\eta_{31}+\eta_{13})(\eta_{12}+\eta_{21})+\cdots.\end{aligned} \tag{2}$$

The conventional contracted notation for the second- and third-order coefficients is used. Therefore, a trigonal crystal has six second-order (usual) constants, and 14 third-order constants.[41]

Now we wish to express the second- and third-order elastic constants of a trigonal crystal in terms of the interatomic potential under the assumption of two-body, central-force interactions between the ions. We exclude here the vibrational part of the free energy, so that the expressions will be valid only at 0°K. The elastic strain-energy density $\Delta\Phi$ is given as the difference in the potential-energy density of the crystal in the deformed and undeformed states. They are, in turn, expressed as the sums of the difference in all the interatomic potentials between ion-pair in the respective states:

$$\begin{aligned}\Phi(\eta)&=\frac{1}{2V_c}\sum_{\binom{m}{\mu}\neq\binom{0}{\nu}}\phi_{\mu\nu}(r_{\mu\nu}{}^{m0})=\frac{1}{2V_c}\sum{}'\phi_{\mu\nu}(r_{\mu\nu}{}^{m0}),\\
\Phi(0)&=\frac{1}{2V_c}\sum{}'\phi_{\mu\nu}(R_{\mu\nu}{}^{m0}),\end{aligned} \tag{3}$$

where V_c is the volume of the unit cell of the trigonal crystal in the unstrained state, $\phi_{\mu\nu}(r_{\mu\nu}{}^{m0})$ is the interaction energy per ion pair between the μth ion in the mth cell and the νth ion in the zeroth cell. $r_{\mu\nu}{}^{m0}$ and $R_{\mu\nu}{}^{m0}$ are the interionic distances in the strained and unstrained states, respectively. Since we define the unit cell of calcite to include only one molecule, $\sum'$ denotes the summations over all the other ions around one Ca ion, one C ion, and three O ions:

$$\Delta\Phi=\frac{1}{2V_c}\sum_{\mathrm{CaCO_3}}{}'(\phi_{\mu\nu}(r_{\mu\nu}{}^{m0})-\phi_{\mu\nu}(R_{\mu\nu}{}^{m0})). \tag{4}$$

Using the relations

$$\begin{aligned}&\mathbf{R}=a_1\mathbf{i}_1+a_2\mathbf{i}_2+a_3\mathbf{i}_3,\\
&R^2=a_\alpha a_\beta\delta_{\alpha\beta},\\
&\mathbf{r}=a_1\mathbf{i}_1'+a_2\mathbf{i}_2'+a_3\mathbf{i}_3'=x_1\mathbf{i}_1+x_2\mathbf{i}_2+x_3\mathbf{i}_3,\\
&r^2=a_\alpha a_\beta I_{\alpha\beta}=x_\alpha x_\beta\delta_{\alpha\beta},\ I_{\alpha\beta}=i_\alpha' i_\beta'=\frac{\partial x_i}{\partial a_\alpha}\frac{\partial x_i}{\partial a_\beta},\\
&\qquad\qquad\alpha, \beta, i=1, 2, 3\end{aligned} \tag{5}$$

the difference in the square of the interionic separation (r^2-R^2) is given by

$$r^2-R^2=a_\alpha a_\beta(I_{\alpha\beta}-\delta_{\alpha\beta}), \tag{6}$$

where $\mathbf{i}_\alpha$, $\mathbf{i}_\alpha'$, etc., are the basic vectors of the lattice in the undeformed and deformed states. One can also express this in terms of the Lagrangian strain components $\eta_{\alpha\beta}$ that are defined in Eq. (1):

$$r^2-R^2=2a_\alpha a_\beta\eta_{\alpha\beta}. \tag{7}$$

In Eqs. (5), (6), and (7) the subscripts, $\mu\nu$, and super-

[40] K. Brugger, Phys. Rev. 133, A1611 (1964).
[41] K. Brugger, J. Appl. Phys. 36, 759 (1965).

TABLE I. Eleven modes and 33 hydrostatic and uniaxial measurements considered ($\alpha_1=0.59576$, $\beta_1=0.80317$, $\alpha_2=0.98512$, $\beta_2=0.17185$, $\alpha_3=0.84294$, $\beta_3=0.53802$, $k=0.705252$, $l=0.71167$).

Mode No. and mode type	Propagation direction N	Polarization direction U	Mode symbol of stress	Compression direction M
1 L[a]	100	100	1 H[b]	all
			1 A[b]	010
			1 B[b]	001
2 S[a]	100	$0\beta_1\bar{\alpha}_1$	2 H	all
			2 A	010
			2 B	001
3 S	100	$0\alpha_1\beta_1$	3 H	all
			3 A	010
			3 B	001
4 QL[a]	010	$0\alpha_2\beta_2$	4 H	all
			4 A	100
			4 B	001
5 QS[a]	010	$0\beta_2\bar{\alpha}_2$	5 H	all
			5 A	100
			5 B	001
6 S	010	100	6 H	all
			6 A	100
			6 B	001
7 L	001	001	7 H	all
			7 A	100
			7 B	010
8 S	001	100	8 H	all
			8 A	100
			8 B	010
9[c] S	001	010	not used	
10 QL	$0kl$[d]	$0\alpha_3\beta_3$	10 H	all
			10 A	100
			10 B	$0lk$
11 QS	$0kl$	$0\beta_3\bar{\alpha}_3$	11 H	all
			11 A	100
			11 B	$0lk$
12 S	$0kl$	100	12 H	all
			12 A	100
			12 B	$0lk$

[a] L = pure longitudinal, S = pure shear, QL = quasilongitudinal, QS = quasishear.
[b] H denotes hydrostatic stress, A and B uniaxial stress.
[c] Mode 9 was not used because of the large internal conical refraction.
[d] This propagation direction was selected normal to the cleavage plane of calcite.

scripts, $m0$, are understood. If we now expand $\Delta\Phi$ in Eq. (4) in a power series in $\frac{1}{2}(r^2-R^2)_{\mu\nu}{}^{m0}$, the second Φ_2 and the third Φ_3 terms can be obtained, respectively, as

$$\Phi_2=\frac{1}{2V_c}\sum_{\mathrm{CaCO_3}}{}'\frac{[\frac{1}{2}(r^2-R^2)_{\mu\nu}{}^{m0}]^2}{2!}D^2\phi_{\mu\nu}(r)_{\mu\nu}{}^{m0}\Big|_{r=R}$$

$$=\frac{1}{4V_c}\sum_{\alpha\beta}\sum_{\alpha'\beta'}\eta_{\alpha\beta}\eta_{\alpha'\beta'}\times[\sum_{\mathrm{CaCO_3}}{}'a_\alpha a_\beta a_{\alpha'}a_{\beta'}D^2\phi_{\mu\nu}(r)\,|_{r=R}], \quad (8)$$

$$\Phi_3=\frac{1}{12V_c}\sum_{\alpha\beta}\sum_{\alpha'\beta'}\sum_{\alpha''\beta''}\eta_{\alpha\beta}\eta_{\alpha'\beta'}\eta_{\alpha''\beta''}\times[\sum_{\mathrm{CaCO_3}}{}'a_\alpha a_\beta a_{\alpha'}a_{\beta'}a_{\alpha''}a_{\beta''}D^3\phi_{\mu\nu}(r)\,|_{r=R}],$$

where $D=(1/r)(d/dr)=(1/a_\alpha a_\beta)\partial/\partial\eta_{\alpha\beta}$. By comparing these expressions in Eq. (8) with the macroscopic definitions of elastic constants, the second-order, $c_{\alpha\beta\alpha'\beta'}{}^0$, and third-order elastic constants, $C_{\alpha\beta\alpha'\beta'\alpha''\beta''}{}^0$, at 0°K are expressed as a function of the interionic potential $\phi_{\mu\nu}(r_{\mu\nu}{}^{m0})$:

$$c_{\alpha\beta\alpha'\beta'}{}^0=\left(\frac{\partial^2\Phi}{\partial\eta_{\alpha\beta}\partial\eta_{\alpha'\beta'}}\right)_{\eta=0}=\frac{1}{2V_c}\times\sum_{\mathrm{CaCO_3}}{}'a_\alpha a_\beta a_{\alpha'}a_{\beta'}D^2\phi_{\mu\nu}(r)_{\mu\nu}{}^{m0}\,|_{r=R},$$

$$C_{\alpha\beta\alpha'\beta'\alpha''\beta''}{}^0=\left(\frac{\partial^3\Phi}{\partial\eta_{\alpha\beta}\partial\eta_{\alpha'\beta'}\partial\eta_{\alpha''\beta''}}\right)_{\eta=0}=\frac{1}{2V_c}\sum_{\mathrm{CaCO_3}}{}'a_\alpha a_\beta a_{\alpha'}a_{\beta'}a_{\alpha''}a_{\beta''}D^3\phi_{\mu\nu}(r)_{\mu\nu}{}^{m0}\,|_{r=R}. \quad (9)$$

Equations (9) and (2) immediately give the Cauchy re-

lations for the second- and third-order elastic constants in a trigonal crystal at 0°K. For the second-order constants these are

$$c_{13}{}^0=c_{44}{}^0, \quad c_{11}{}^0=3c_{12}{}^0, \tag{10}$$

and for the third-order constants

$$\begin{aligned}&C_{133}{}^0=C_{344}{}^0, \quad C_{134}{}^0=-C_{444}{}^0,\\ &C_{114}{}^0=3C_{124}{}^0, \quad C_{113}{}^0=C_{155}{}^0=3C_{123}{}^0=3C_{144}{}^0,\\ &C_{111}{}^0+5C_{112}{}^0=3C_{222}{}^0, \quad C_{111}{}^0+C_{112}{}^0=C_{113}{}^0+C_{222}{}^0.\end{aligned} \tag{11}$$

Hence, under the central-force assumption, there are only four independent second-order ($c_{11},c_{13},c_{14},c_{33}$) and six independent third-order ($C_{111},C_{112},C_{114},C_{133},C_{134},C_{333}$) constants for a trigonal crystal. At temperatures other than 0°K, of course, the contribution from the vibrational free energy comes into play, so that these relations in Eqs. (10) and (11) are no longer valid even under the two-body, central-force model.[10,11]

B. Relations between Elastic Constants and Sound Velocity

For the propagation of sound waves at zero stress, substitution of plane-wave solutions into the equations of particle motion gives eigenvalue equations for the sound velocity:

$$\begin{aligned}&\rho V^2U_i=\lambda_{ij}U_j,\\ &\lambda_{ij}=c_{ikjl}N_kN_l,\end{aligned} \tag{12}$$

where ρ is the density of the solid under consideration, V is the velocity of ultrasound, and U_i and N_i are the components of unit vectors in the directions of polarization and propagation, respectively. After fixing the propagation directions of the sound waves, one can obtain the eigenvalues for ρV^2, and hence the relations between ρV^2 and the second-order elastic constants c_{ikjl}. Explicit expressions for ρV^2 for a trigonal crystal can thus be found[42] for the modes which are of experimental interest (Table I).

In the strained state where sound waves propagate through the stressed solid, the third-order elastic constants C_{ijk} come into the equations of particle motion when the strains are finite.[8,19,43] The corresponding expressions for ρV^2 are functions of the C_{ijk}'s; and ρ and V are now the density and velocity in the strained crystal, respectively. According to the definitions of elastic constants,[40] the C_{ijk}'s are derivatives of the effective second-order elastic constants with respect to the pertinent Lagrangian strain component. Hence, the change in apparent ρV^2 with stress p is more directly related to the third-order elastic constants than ρV^2 itself. However, it is not easy to take the derivative of Eq. (12) with respect to stress, because the polarization and propagation directions are rotated and the density and the path length are also changed when stress is applied. To allow for this, Thurston and Brugger[44] have utilized such convenient parameters as the "natural velocity" W, the density ρ_0 in the unstrained state, and the expression w_{ij} corresponding to λ_{ij} but independent of the rotation of the deformed material. W is defined as twice the path length in the unstressed state divided by the round-trip transit time of sound wave in the stressed state. Thus Eq. (12) becomes

$$\rho_0W^2U_i=w_{ij}U_j. \tag{13}$$

After taking derivatives of both sides of Eq. (13) with respect to stress p and computing the term $-[\partial(\rho_0W^2)/\partial p]$, they have arrived at very useful general expressions connecting third-order elastic constants to the natural velocity. For hydrostatic compression

$$\begin{aligned}&-[\partial(\rho_0W^2)/\partial p]_{p=0}=1+2wF_{\rm HC}+G_{\rm HC},\\ &F_{\rm HC}=s_{aars}{}^TU_rU_s,\\ &G_{\rm HC}=s_{aauv}{}^TC_{uvprqs}N_pN_qU_rU_s\\ &\quad=-B_{prqs}N_pN_qU_rU_s,\\ &-B_{prqs}=s_{iiuv}{}^TC_{uvprqs},\end{aligned} \tag{14}$$

and for uniaxial compression

$$\begin{aligned}&-[\partial(\rho_0W^2)/\partial p]_{p=0}=2wF_{\rm UC}+G_{\rm UC},\\ &F_{\rm UC}=s_{abrs}{}^TM_aM_bU_rU_s,\\ &G_{\rm UC}=s_{abuv}{}^TC_{uvprqs}M_aM_bN_pN_qU_rU_s,\end{aligned} \tag{15}$$

where $w=(\rho_0W^2)_{p=0}=(\rho V^2)_{p=0}=c_{prqs}{}^SN_pN_qU_rU_s$; s^T are the isothermal second-order compliance constants; and M_i are the components of the unit vector in the direction of the uniaxial stress (which is usually taken

TABLE II. (A) The chemical compositions, and (B) thicknesses and linear thermal-expansion coefficients of calcite specimens used.

(A) Main impurities of the calcite specimens, in weight%.

Al	Si	Mn	Sr	Mg	Fe	Ni	Cu
0.1	0.06	0.038[a]	0.02	0.015[a]	0.006	0.004	0.002

(B) Thicknesses at 0°C and thermal-expansion coefficients at room temperature.

Specimen no. and direction	Thickness at 0°C (cm)	Linear thermal-expansion coefficient[b] (per °C)
spec 1.		
100(X)	2.07264	-4.9×10^{-6}
010(Y)	1.80322	-4.9×10^{-6}
001(Z)	1.91371	25.1×10^{-6}
spec 2.		
100(X)	2.22961	-4.9×10^{-6}
0lk	2.23897	
0kl[c]	1.97911	10.8×10^{-6}

[a] By flame emission; all the others by spectrographic powder-arc method.
[b] J. B. Austin, H. Saïni, and R. H. H. Pierce, Phys. Rev. **57**, 931 (1940).
[c] This direction is normal to the cleavage plane of calcite.

[42] H. J. McSkimin, J. Acoust. Soc. Am. **34**, 1271 (1962).
[43] A. Seeger and O. Buck, Z. Naturforsch, **15a**, 1056 (1960).
[44] R. N. Thurston and K. Brugger, Phys. Rev. **133**, A1604 (1964).

as perpendicular to the propagation direction N). Thus, a linear combination of third-order elastic constants has been directly related to the change of the natural velocity W with stress p. For a trigonal crystal, $-[\partial(\rho_0 W^2)/\partial p]_{p=0}$ must be measured for at least 14 independent cases to determine the complete set of the constants. Explicit expressions for $-[\partial(\rho_0 W^2)/\partial p]_{p=0}$ have been presented by Thurston, McSkimin, and Andreach[30] for α-quartz crystals for a set of 34 independent cases: 10 cases for 10 modes under hydrostatic pressure and 24 cases for 12 modes under uniaxial stress. In the present experiments, 33 cases were considered: one hydrostatic and two uniaxial cases for each of 11 independent modes. Furthermore, the propagation direction for modes 10, 11, and 12 (see Table I) was chosen perpendicular to a cleavage plane in order to obtain a well-defined crystal orientation. As a result, 24 (modes 1–8) of the 33 cases which we consider are equivalent to those discussed by Thurston *et al.*

III. EXPERIMENTAL PROCEDURE

A. Specimen Preparation

Calcite has the same composition ($CaCO_3$) as argonite, but trigonal instead of orthorhombic crystal symmetry. Its structure is related to the NaCl structure, but its lattice compressed along one of the threefold, body-diagonal axes to accommodate the large planar CO_3 ions. The conventional cleavage unit-cell contains four molecules as does the NaCl structure and, though not a true cell, it is often conveniently referred to for many experimental purposes. Figure 1 illustrates the arrangement of calcium, carbon, and oxygen atoms in a cleavage rhombohedral pseudocell.

Several natural calcite crystals of optical quality were supplied by the National Bureau of Standards for the present work. Chemical analysis of them was performed by flame-emission, powder-arc spectrographic methods with the results shown in Table II A. Three cubic specimens (specimens 1, 2, and 3) were cut from one large crystal (1.5×1.5×3 in.) with a wafering diamond saw. The cutting stage permitted rough orientation of the faces of the specimens. The three pairs of cube faces of specimen 1 are each perpendicular to the X, Y, and Z axes of the calcite lattice, while specimen 2 has one pair normal to X axis, another parallel to one cleavage plane, and the third selected normal to the first two. Specimen 3 is identical in orientation and size with specimen 1 and was used only to examine the sensitivity of the two-specimen method. The Cartesian coordinate system was chosen by the convention that the Z axis coincides with the optic triad axis, the X axis is parallel to one of the twofold symmetry axes, and the Y axis completes the right-handed coordinate system as shown in Fig. 1. These specimens were then accurately oriented and flattened. First they were polished flat to about 5×10^{-4} in. by hand on a glass plate with aluminum-oxide powder (9.5 μ) and ethyl alcohol. Also, their orientations were checked by the x-ray back-reflection method, until the desired orientation was obtained within $\pm0.1°$. Then the crystals were mounted on a cylindrical, aluminum polishing holder with previously machined flat edges and a thickness slightly larger than the specimen. This whole assembly was polished on a granite plate with polishing oil and aluminum oxide until the specimen was flat and parallel to $\approx3\times10^{-5}$ in. After the final polishing, the orientations were checked and the thickness and flatness were measured with a Brown and Sharp electronic thickness gauge. Table II B shows the thicknesses and orientations of the two specimens (1 and 2) together with their linear thermal-expansion coefficients in the directions of sound-wave propagation.

Although plastic deformation due to slip can occur in calcite at room temperature, the slip systems are few[38] and the mobilities of dislocations are very low.[45] The critical stress is usually much lower for twinning than for slip near room temperature.[38] No dislocation motion was observed in calcite by an etch-pit technique near and below room temperature under the usual conditions.[45,46] In order, therefore, to avoid the difficulty of dislocation-modulus change due to unpinning of dislocations, the maximum uniaxial compression stress was kept below 50 kg/cm^2 in these experiments. This approximately corresponds to the minimum shear stress required for twinning at room temperature. Thus, unlike the case of metals,[28] a nonlinear change of sound velocities with uniaxial stress was not detected in this stress range.

B. Temperature and Stress Measurement

Temperature measurements were made with a calibrated Chromel-Advance thermocouple attached to the specimen surface. This thermocouple has a high thermoelectromotive force (about 50 μV/°C). The temperature of the specimen was varied by a small heating coil placed around the specimen inside a temperature bath. The voltage produced by the thermocouple was partially balanced with a Rubicon model No. 2768 potentiometer, and the unbalanced signal ($\lesssim10$ μV) was amplified (Leeds and Northrup DC amplifier) and then fed into a chart recorder (Hewlett Packard model No. 7100B/7101B), where the full-scale deflection (20 cm) corresponded to 10-μV imbalance in the potentiometer. The resolution of the temperature measurement was $\pm1\times10^{-3}$°C for hydrostatic pressure and zero-stress runs; and $\pm3\times10^{-3}$°C for uniaxial compression runs. In the case of hydrostatic pressure measurements, the temperature was always read after thermal equilibrium had been reached between the specimen and its ambient.

Specimens were compressed either hydrostatically or uniaxially to cause a variation of sound velocity with stress. The hydrostatic pressure was applied up to 120 kg/cm^2 in steps of 10 kg/cm^2 by using gaseous nitrogen

[45] R. E. Keith and J. J. Gilman, Acta Met. 8, 1 (1960).
[46] J. J. Gilman (private communication).

as a pressure agent in a pressure vessel that was immersed in an ice bath. A Heise Bourdon tube pressure gauge with a capacity of 150 kg/cm^2 was used to read the applied pressure to ± 0.05 kg/cm^2. For the uniaxial stress measurements a small hydraulic compression machine was used with a dial gauge of about 100 kg/cm^2 in capacity and an accuracy of ± 1 kg/cm^2. The uniaxial stress was changed between 0 kg/cm^2 and about 50 kg/cm^2 in steps of 5 kg/cm^2. To make the stress uniform, a specially designed compression jig allowed smooth rotations of the upper loading plate and prevented oblique loading. Indium shims were inserted between the specimen and the upper and lower loading plates. The jig was placed in an ice bath at 0°C to minimize temperature fluctuations of the specimen.

C. Sound-Velocity Measurements

Calcite crystals are fragile, so only relatively small static stresses can be applied to them. To detect the small velocity changes that result it is necessary to use methods of the highest possible sensitivity. For absolute sound-velocity measurements, four different methods were used to accurately determine the second-order elastic constants of calcite and to provide cross-checks among the methods. The methods are: (1) direct pulse echo,[47] (2) two-echo interference,[35,36] (3) gated-carrier echo-continuous-wave interference, and (4) improved gated-carrier pulse superposition.[33,48] For measuring velocity changes with temperature or stress, the sensitivities of the following four methods were studied: (2), (3), (4), and (5) the two-specimen interference method.[28,49] Method (4) was found to have the highest sensitivity. One set of equipment (A) was built for four methods [(1), (2), (3), and (5)], and another set (B) was independently prepared for method (4).

The apparatus (A) is essentially a gated-carrier, pulsed interferometer as used by Williams and Lamb[35] and developed by Colvin.[36] The continuous rf carrier wave generated by the frequency synthesizer (General Radio 12-MHz synthesizer, type 1163-A5C) is fed into the gated-amplifier circuit, where the continuous wave is gated at two amplification stages by means of positively biased rectangular pulses from the dc pulse generated at a low repetition rate ($\approx$300 cps). The gated, flat-topped rf pulses with fixed pulse width are then sent into the balancing network (Arenburg WB-100), the purpose of which is twofold: to improve the rf pulse shape and to increase the ratio of echo to direct-pulse amplitude. The rf pulse from the balancing network is used to excite the quartz transducer bonded to the calcite specimen. Echoes received by the same transducer are then transferred via the balancing network to the dual-trace preamplifier (type 1A1) of a Tektronix 547 oscilloscope. The circuits for the gated amplifier and the dc pulse generator used here are exactly the same as described in Colvin.[36] But in this system a dc bias voltage was employed to provide two different dc pulse levels for the two stages to increase the signal-to-noise ratio. Also, the dc pulse generator was modified to generate either one or two pulses.

In method (1), several round-trip transit times between successive echoes are measured to determine the average value. The measurements are made directly on an oscilloscope that is calibrated with a time-mark generator (Tektronix 180A). Method (2) is fully described elsewhere,[35,36] but in this experiment the first echo of the second pulse is superposed upon an echo of the first pulse, where the two pulses are separated as far in time as possible while still maintaining the destructive interference condition between the echoes. In method (3)[50] the continuous rf signal from the frequency synthesizer is sent to one channel of the oscilloscope preamplifier. The second channel of the preamplifier receives a direct pulse and its echo train detected by the transducer. The two signals are added algebraically inside the preamplifier and displayed on the oscilloscope. Six or seven interference frequencies, at which one selected echo is exactly in antiphase with the continuous wave, are measured with the synthesizer. This is repeated for two selected successive echoes in this method. Although the continuous wave and the gated pulse are generated by the same oscillator, the effects of gating and differing path lengths may cause some phase differences between them. Therefore, in this method, one round-trip transit time is calculated as the difference of the two delay times for the two successive echoes. This apparatus (A) can also be used for the two-specimen interference method (5), as developed by Espinola and Waterman,[49] and applied by Hiki and Granato.[28] However, this method is only applicable to the relative measurements of velocity.

The pulse-superposition method of McSkimin[33,51] has become most widely used for measuring both absolute and relative sound velocities.[19,21–23,27,30] However, the gated-carrier pulse-superposition method,[33] in which the rf pulses with different initial phases are generated by gating a coherent continuous wave, is less frequently used[33] than the pulsed-oscillator pulse-superposition method,[51] in which identical but not phase-coherent rf pulses are produced. In the present work an improved gated-carrier pulse-superposition method (4) was also used. The apparatus (B) for this method was developed by J. Holder[48] of this laboratory, and procedures for obtaining the optimum sensitivities for calcite were developed by the author. Its circuit diagram, however, is essentially the same as McSkimin's,[33] including the frequency modulation technique for improved sensi-

[47] H. B. Huntington, Phys. Rev. **72**, 321 (1947).
[48] J. Holder (to be published).
[49] R. P. Espinola and P. C. Waterman, J. Appl. Phys. **29**, 718 (1958).
[50] This method appears to be somewhat analogous to those described in H. J. McSkimin, J. Acoust. Soc. Am. **30**, 314 (1958); J. de Klerk, Rev. Sci. Instr. **36**, 1540 (1965).
[51] H. J. McSkimin and P. Andreatch, Jr., J. Acoust. Soc. Am. **41**, 1052 (1967).

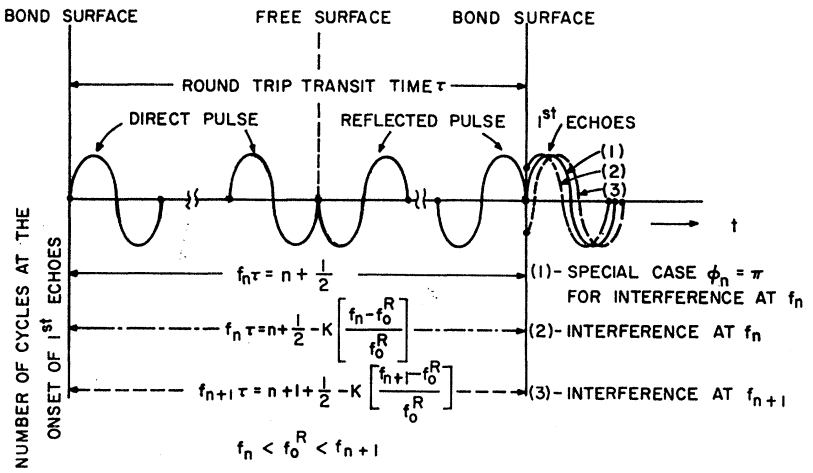

FIG. 2. Phase difference and number of cycles of rf frequency after one round-trip transit time at two interference conditions f_n and f_{n+1}. Since the magnitude of $K[(f_n-f_0{}^R)/f_0{}^R)]$ or $K[(f_{n+1}-f_0{}^R)/f_0{}^R]$ is less than 1.5×10^{-2}, the phase difference from the special case ($\phi_n=\pi$, phase-shift correction term is zero) for these interference conditions is very small and the number of carrier cycles is different only by less than 1.5×10^{-2} from $(n+\frac{1}{2})$ cycles of the special case. From this figure it is clearly known that the phase correction term can be neglected to determine the integer value n.

tivity. The carrier frequency is modulated by coupliug a low modulation frequency ac signal (40–60 cps, 3 V) from an external source to the frequency synthesizer. The amplitude of the summed echoes is oscillated at twice the modulation frequency as the amplitude moves along the "resonance curve"[33] of echo amplitude versus carrier frequency, because the modulated carrier frequency oscillates about the constructive interference frequency of the superposed echoes. (The modulation range of the carrier frequency is about ±100 cycles.) The echo oscillation is an exactly symmetric, sinusoidal curve on an oscilloscope when the carrier frequency is set correctly to the frequency of the "resonance peak" (this is the desired critical interference frequency) provided that the "resonance curve" is symmetric around the peak frequency. Since the echo shapes were not exactly rectangular and each echo contained only 10–20 cycles (the pulse width was variable over 1–2 μsec in this method), the repetition rate frequency must be adjusted as the carrier frequency changes in order to keep the phase condition critically matched. Discussion of this is given in the Appendix.

In the pulse-superposition method a large number of echoes are superposed upon each other and even high-number echoes with relatively small amplitudes can influence the interference condition. The deviation of the echo envelope from the exponential attenuation made it necessary to check the possible existence of an extra phase change for these echoes due to some distortion upon reflection. To do this, interference frequencies were measured at the same temperature for various sets of superposed echoes (some multiple p[33] of round-trip delay time=2, 3, 4, 5, 6, 7) and were found to be the same within experimental error.

An X-cut or Y-cut tuned quartz transducer (10 Mc/sec) of $\frac{3}{8}$-in. diam was cemented to the specimen surface with salol, and was operated near the resonance frequency of the transducer. In the absolute-velocity measurements, several interference frequencies were picked up near the resonance frequency, while in the relative measurements, the change in the interference closest to the resonance frequency was followed as temperature or stress changed.

Let us now turn to the principle of the absolute-velocity measurement. We consider only the principle of method (2), because the principles for methods (2), (3), and (4) are essentially the same. When a destructive interference condition is exactly satisfied for one round-trip delay time, the phase difference between the two successive echoes is an odd integer times π:

$$2\pi f_n\tau-\phi_n-\pi=(2n-1)\pi, \tag{16}$$

which is equivalent to

$$f_n\tau=(n+\tfrac{1}{2})-K[(f_n-f_0{}^R)/f_0{}^R], \tag{17}$$

because the phase angle ϕ_n on reflection at the transducer face of the specimen is given by[35]

$$\phi_n=\pi[1-2K(f_n-f_0{}^R)/f_0{}^R] \tag{18}$$

for the interference near the transducer resonance frequency $f_0{}^R$, where f_n is the carrier interference frequency, τ is one round-trip delay time of the echo, π is the phase change caused at the free surface of the specimen, n is an integrer associated with the number of rf cycles for one round trip, and K is the ratio of the acoustic impedance of the transducer to that of the specimen. Since the central two interference frequencies f_n and f_{n+1} are always chosen within 100 kc from $f_0{}^R$ ($\approx10^7$ cps) in this experiment, $K[(f_n-f_0{}^R)/f_0{}^R]$ in Eq. (17) is less than 1.5×10^{-2} ($K\lesssim1.5$ for calcite). For the next higher interference frequency f_{n+1} we have

$$f_{n+1}\tau=(n+1+\tfrac{1}{2})-K[(f_{n+1}-f_0{}^R)/f_0{}^R] \tag{19}$$

and $K[(f_{n+1}-f_0{}^R)/f_0{}^R]$ is again very small. Figure 2 shows the difference of the number of rf cycles, which is almost one, and of the phase changes for one round trip for these two interference conditions. Since n is a large integer (about 100 for shear waves and about 50 for longitudinal waves), the phase-correction term in Eqs. (17) and (19) can be safely neglected for the experi-

mental determination of n and $n+1$:

$$n+\tfrac{1}{2}\approx f_n\tau, \tag{20}$$

$$n+1+\tfrac{1}{2}\approx f_{n+1}\tau. \tag{21}$$

Then, since $\Delta f_n\equiv f_{n+1}-f_n$, we have[52]

$$n+\tfrac{1}{2}\approx f_n/\Delta f_n, \tag{22}$$

and when this is combined with Eq. (17)[52]

$$\tau\approx 1/\Delta f_n - K(1/f_0{}^R - 1/f_n). \tag{23}$$

There is no ambiguity for expressions (22) and (23) if the correct integer value for n can be selected; but even if ambiguity remains, the maximum error for n and τ caused by the neglection of the phase-correction term should be less than about $\frac{2}{5}\times 10^{-3}$.

On the other hand, subtraction of Eq. (17) from Eq. (19) gives

$$\tau(f_{n+1}-f_n)=1-(K/f_0{}^R)(f_{n+1}-f_n), \tag{24}$$

and from this,

$$n+\tfrac{1}{2}=(f_n/\Delta f_n)-K, \tag{25}$$

$$\tau=1/\Delta f_n - K/f_0{}^R. \tag{26}$$

In Eqs. (25) and (26) the ratio of the second (phase-correction) term to the first term is quite large (1–2%) as compared with that ($\approx\frac{2}{5}\times 10^{-3}$) in the original Eqs. (17) and (19), and therefore Eqs. (25) and (26) have an unreasonably large contribution from the phase-shift correction term. However, these are invalid expressions derived from the subtraction between two almost equal quantities, both having errors. This has not been pointed out in the literature.[35,36] In fact, Eq. (24) means that one tries to determine τ using only one cycle with a large uncertainty $(K/f_0{}^R)(f_{n+1}-f_n)\approx 1.5-2\times 10^{-2}$. The correction term $K[(f_n-f_0{}^R)/f_0{}^R]$ is small compared to $(n+\frac{1}{2})$ cycles in Eq. (17), but the corresponding correction term $(K/f_0{}^R)(f_{n+1}-f_n)$ is not negligibly small compared to one cycle in Eq. (24). As a result, we have to use Eqs. (22) and (23) to compute n and τ. In the actual practice, when Eqs. (25) and (26) were used in methods (2), (3), and (4), the resultant transit times were always smaller by 1–2% than those measured by the direct pulse-echo method (1), whereas Eqs. (22) and (23) gave a very small difference. From Eq. (23) the sound velocity can be calculated by knowing the thickness of the specimen.

A knowledge of the change in the natural velocity W with stress p, i.e., $-[\partial(\rho_0W^2)/\partial p]_{p=0}$ is necessary to determine third-order elastic constants. Since the natural velocity is experimentally known to depend linearly on stress, the expression

$$\frac{1}{(\rho_0W^2)_{p=0}}\left[\frac{\partial(\rho_0W^2)}{\partial p}\right]_{p=0}=\frac{2}{W_0}\left(\frac{\partial W}{\partial p}\right)_{p=0} \tag{27}$$

is equivalent to

$$(\rho_0W^2)'_{p=0}=\frac{2w}{p}\frac{\Delta W}{W_0}=\frac{2w}{p}\frac{\Delta\tau}{\tau_0}, \tag{28}$$

where W_0 and τ_0 are the natural velocity and the round-trip transit time at $p=0$, and $w=(\rho_0W^2)_{p=0}$ as given before. Using Eq. (17), Eq. (28) may be written within experimental accuracy as

$$(\rho_0W^2)'_{p=0}=(2w/p)(\Delta f/f_0). \tag{29}$$

Similarly, the temperature dependence of the natural velocity is given by

$$\frac{1}{W}\frac{\partial W}{\partial T}=\frac{1}{\Delta T}\frac{\Delta f}{f_0}. \tag{30}$$

In Eqs. (29) and (30), f_0 is the reference-interference frequency either at zero stress, or at the reference temperature, and Δf is the change with either stress or temperature. Consequently, it is only necessary in the anharmonic measurement of elastic constants to measure the fractional change in the interference frequency with either stress or temperature. This cannot be conveniently done using the true velocity V, because $\Delta V/V_0$ is not proportional to $\Delta f/f_0$.

The accuracy of absolute-velocity measurements in terms of the reproducibility of τ was found to be as follows: 6×10^{-3} for method (2), 2×10^{-3} for method (3); a little better than 2×10^{-4} for method (4); and 1×10^{-2} for method (1). The accuracy of measurement of the interference frequencies, however, was 1×10^{-5} for

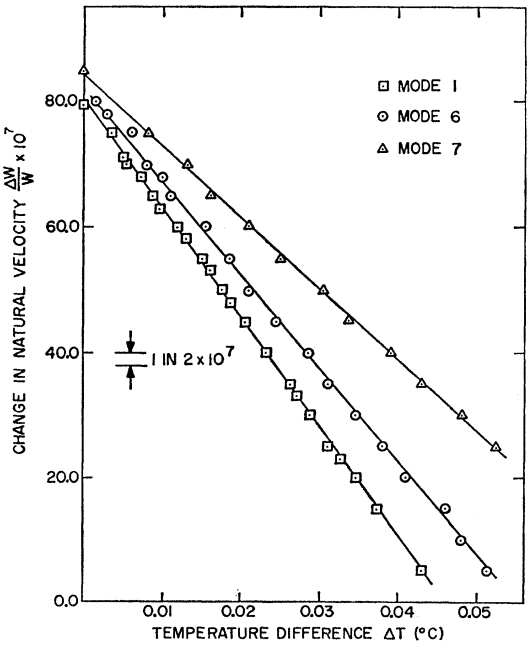

FIG. 3. Change in natural velocity with temperature for modes 1, 6, and 7.

[52] This expression is essentially equivalent to $n=f_n/\Delta f_n$ used for the constructive interference by H. J. McSkimin in Ref. 54. Discussion about this expression and Eq. (23) will be given in a separate short note.

TABLE III. Second-order elastic constants c_{ij} (in 10^{11} dyn/cm^2) and compressibilities κ_{vol}, κ_{II}, $\kappa_{\perp}$ (in 10^{-12} cm^2/dyn) of calcite at room temperature.[a]

	Present work					Pulse-echo	Other methods (isothermal)			
	isothermal 4	method 4	method 3	method 2	method 1	method[b]	c	d	e	f
c_{11}	14.523	14.535	14.291	14.706	14.339	14.45	13.74	13.71	16.22	16.95
c_{12}	5.486	5.501	5.383	5.560	5.395	5.71	4.40	4.56	4.53	5.93
c_{13}	5.249	5.280	4.918	5.121	5.659	5.34	4.50	4.51	6.35	7.25
c_{14}	−2.032	−2.031	−2.037	−2.057	−2.011	−2.05	−2.03	−2.08	−3.12	−2.87
c_{33}	8.433	8.564	8.474	8.656	8.481	8.31	8.01	7.97	9.77	10.46
c_{44}	3.290	3.289	3.403	3.402	3.350	3.265	3.42	3.42	4.29	4.14
		Present adiabatic 4	g	h	i	b	c	d	e	f
κ_{vol}		1.386	1.367	1.35	1.39	1.396	1.53	1.55	1.22	1.103
κ_{II} (parallel to Z axis)		0.818	0.822	···	···	0.858	0.883	0.882	0.66	0.625
$\kappa_{\perp}$ (perpendicular to Z axis)		0.284	0.273	···	···	0.269	0.337	0.330	0.28	0.239

[a] Maximum error due to linear extrapolation to room temperature was less than 0.05%. $\kappa_{vol}=2(s_{11}+s_{12})+4s_{13}+s_{33}$, $\kappa_{II}=2s_{13}+s_{33}$, $\kappa_{\perp}=s_{11}+s_{12}+s_{13}$.
[b] L. Peselnick and R. A. Robie, J. Appl. Phys. **34**, 2494 (1963).
[c] J. Bhimasenachar, Proc. Indian Acad. Sci. **22**, 199 (1945).
[d] W. Voigt, *Lehrbuch der Kristallphysik* (B. G. Teubner, Berlin, 1910), p. 754.
[e] Reference 60.
[f] Reference 61.
[g] P. W. Bridgman, Am. J. Sci. **10**, 483 (1925).
[h] E. Madelung and R. Fuchs, Ann. Phys. **65**, 289 (1921).
[i] L. H. Adams, E. D. Williamson, and J. Johnston, J. Am. Chem. Soc. **41**, 12 (1919).

method (2), 3×10^{-6} for method (3), and 2×10^{-7} for method (4). Therefore, only method (4) had smaller errors than the phase-shift correction term ($\approx\frac{2}{5}\times10^{-3}$) neglected in Eq. (22).

The sensitivities of methods (2), (3), (4), and (5) in the relative-velocity measurements were also investigated for the temperature dependence of the natural velocity for various modes. The average values and ranges obtained are as follows: 2×10^{-5} (1×10^{-5}—1×10^{-4}) for method (2); 2×10^{-6} (5×10^{-7}—5×10^{-6}) for method (3); 2×10^{-7} (5×10^{-8}—3×10^{-7}) for method (4); and 2×10^{-5} (5×10^{-6}—5×10^{-5}) for method (5). In Fig. 3 the very good sensitivity of method (4) can be seen for three modes. Note that these accuracies and sensitivities are relevant only to the measurements on calcite crystals, as the sensitivity depends strongly on the attenuation of the sample.[37] The attenuation envelope for calcite was never of the smooth, exponential type, and the attenuation increased with applied stress which reduced considerably the sensitivity of the two-specimen method (5) as compared with the result (5×10^{-6}) obtained by Hiki and Granato.[28] Internal-conical refraction was also observed in calcite for the pure modes 8 and 9 with the propagation direction along the threefold axis.[53] The semiangle of the refraction cone was so large (31°40′) for calcite in comparison with other trigonal crystals (quartz, 17°13′; sapphire, 9°3′) that mode 9 could not be used even with good bond because of the very small deteriorated echoes.

To test the applicability of the improved pulse-superposition method (4) to absolute and relative velocity measurements, the absolute velocity at room temperature and the temperature dependence of the elastic constants at 0°C in germanium were measured for one particular mode **N**=[001], **U**=[001]. The results were 4.9120×10^5 cm/sec for the longitudinal velocity and -0.1182×10^{-3}/°C for $(1/c_{11})(dc_{11}/dT)$. This temperature dependence compares quite well with the measurements (-0.11×10^{-3}/°C and -0.12×10^{-3}/°C) [54] made at 0°C by Fine and McSkimin, respectively, which are cited by Leibfried and Ludwig.[55] The absolute velocity agrees within 0.04% with the value of McSkimin *et al.*: 4.9138×10^5 cm/sec.[56]

The effects of the transducer and its bond on the velocity and temperature dependence of the interference frequency were also checked by method (4) for one longitudinal mode (mode 1) of calcite. A second transducer with almost the same resonance frequency was placed on the opposite crystal surface. No large change in the echo transit time due to the echo penetration was observed, but errors caused by resonance between the two transducers prevented an exact estimation of the phase shifts. The effect on the temperature dependence lay within the experimental error.

The following values were used for the density of calcite ρ_c, the density of quartz ρ_T, and the sound velocities in X- and Y-cut quartz crystals V_L, V_T (all at room temperature): $\rho_c=2.712$ g/cc,[57] $\rho_T=2.6485$ g/cc, $V_L=5.749\times10^5$ cm/sec, and $V_T=3.918\times10^5$ cm/sec.[42] To get ρ_c at 0°C an extrapolation based on the volume expansion coefficient (13.14×10^{-6}/C°) [58] was used. The resonance frequencies of the transducers (measured at room temperature) were also extrapolated to °0C using McSkimin's data[59] (-2.006×10^{-5}/C° for X cut, and 8.482×10^{-5}/C° for Y cut).

[53] P. C. Waterman, Phys. Rev. **113**, 1240 (1959).

[54] H. J. McSkimin, J. Appl. Phys. **24**, 988 (1953); M. E. Fine, *ibid.* **26**, 862 (1955).
[55] G. Leibfried and W. Ludwig, Solid State Phys. **12**, 275 (1961).
[56] H. J. McSkimin and P. Andreatch, Jr., J. Appl. Phys. **34**, 651 (1963).
[57] D. L. Graf, Am. Mineralogist **46**, 1283 (1961).
[58] J. L. Rosenholtz and D. T. Smith, Am. Mineralogist **34**, 846 (1949).
[59] H. J. McSkimin and P. Andreatch, J. Acoust. Soc. Am. **34**, 906 (1962).

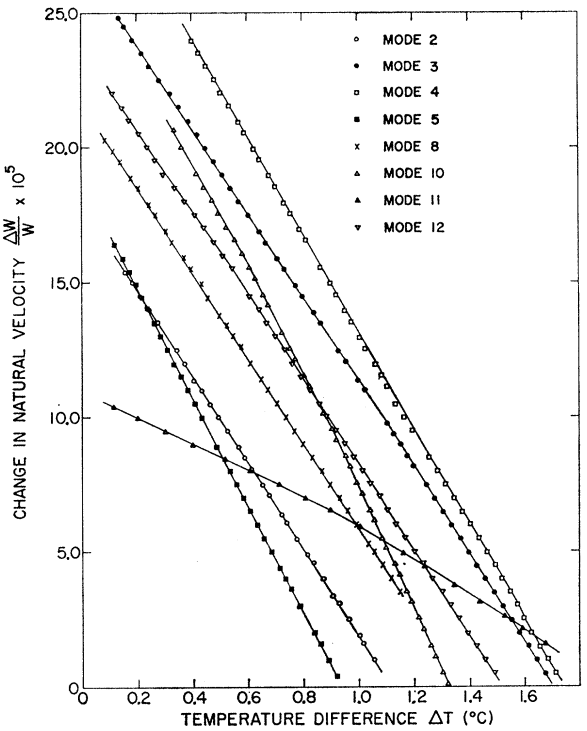

FIG. 4. Change in natural velocity with temperature for modes 2, 3, 4, 5, 8, 10, 11, and 12.

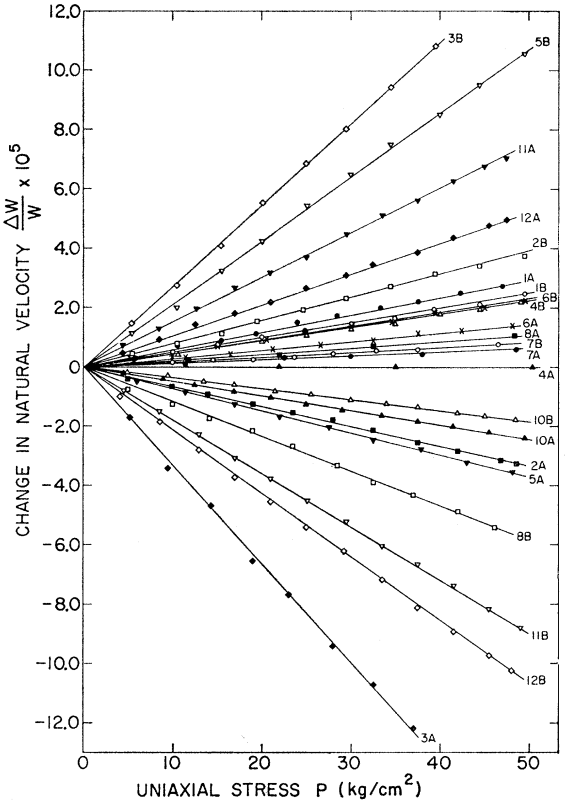

FIG. 5. Change in natural velocity with uniaxial compressive stress.

IV. EXPERIMENTAL RESULTS

A. Experimental Data

The adiabatic second-order elastic constants c_{ij}, and the compressibilities κ_{vol}, κ_{11}, $\kappa_{\perp}$, of calcite were measured at 0°C by the four methods (1), (2), (3), and (4), using the eleven propagation and polarization modes listed in Table I. The results were extrapolated to room temperature and are given in Table III together with the isothermal constants calculated from the results of method (4) and the data of other investigators. The four sets are in good agreement with each other, but the values from method (4) have least errors ($\approx 2\times10^{-4}$). Note that the values of c_{11}, c_{12}, c_{13}, and c_{33} are consistently higher and more mutually similar for pulse-echo methods than the others (Table III).

Figures 3 and 4 show the temperature dependences of the natural velocities for the various modes. These measurements were done for the temperature range of 0 to 2°C with method (4). The deviations of the plotted points from the smooth curves are very small. Even for this small range of temperature, nonlinear dependence was observed for modes 10 and 11 (Fig. 4).[59] Therefore, one must be careful to choose an appropriate temperature coefficient when a temperature correction is made. [The stress effect is usually two orders of magnitude smaller in $(kg/cm)^{-1}$ than the temperature effect in $°C^{-1}$.] As another example, the temperature coefficient of the natural velocity was -1.837×10^{-4}/°C at 0°C and -2.045×10^{-4}/°C at room temperature for mode 4.

One hydrostatic and two uniaxial compression measurements were performed for each of the eleven modes also using method (4). The results for the dependence of the natural velocity on uniaxial stress for 22 cases is shown in Fig. 5, and on hydrostatic pressure for 11 cases in Fig. 6. The points near the origins of the graphs deviate from straight lines (probably because of changes in the bond properties during initial loading), so specimens with transducers attached were prestressed several times prior to making measurements. Because a large increase in temperature (2–3°C) accompanied hydrostatic compression of the specimens, the interference frequencies were measured after the temperature had stabilized near the initial temperature. (The temperature dependence of interference frequencies was different under stress from that under zero stress and it was not linear even for a range of 2 or 3°C.) In the uniaxial stress runs, the specimen temperature changed only 0.2 to 0.3°C for the entire stress range. In the uniaxial velocity measurements the stress coefficients for each shear mode except mode 6 were split into positive and negative values according to the stress directions (A or B), whereas for the longitudinal modes (1, 4, 7, 10) they had only one sign regardless of the stress direction (Fig. 5). In the hydrostatic velocity measurements, on the other hand, all longitudinal modes had rather large,

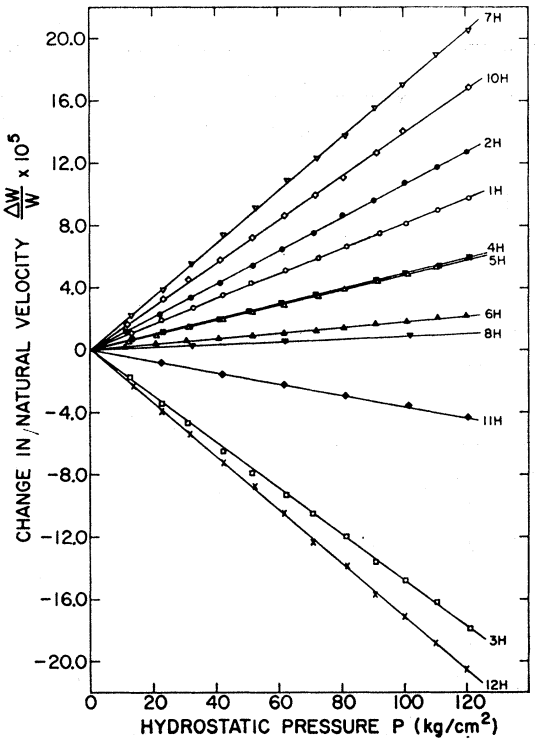

FIG. 6. Change in natural velocity with hydrostatic pressure.

positive values for the coefficients but negative coefficients were also observed for the three shear modes $3H$, $11H$, $12H$ (Fig. 6).

B. Analysis of the Data and the Third-Order Elastic Constants

If the thermal-expansion coefficients of calcite are known, the temperature dependence of the second-order elastic constants at 0°C can be calculated from the data in Figs. 3 and 4. The fractional temperature change of ρV^2 for any mode is given by

$$\frac{1}{\rho V^2}\frac{\partial(\rho V^2)}{\partial T}=2A+2\alpha-\gamma, \qquad (31)$$

where A is the temperature dependence of the natural velocity for that mode at 0°C, α is the linear thermal expansion coefficient in the direction of sound-wave propagation, and γ is the volume thermal-expansion coefficient. The logarithmic temperature dependences of c_{ij} are thus calculated and given in Table IV, along with the data by Reddy and Subrahmanyam[60] and Ramamurthy and Reddy,[61] which were converted from $(1/s_{ij})\times(\partial s_{ij}/\partial T)$. Although the present results refer to 0°C, while the latter two are the average, respectively, between 0 and 200°C and between 0 and 30°C, nevertheless one can readily see the large discrepancies between the three measurements; all the temperature coefficients are negative for the present measurement, whereas they are all positive for the data by Reddy and Subrahmanyam and large positive and negative for those by Ramamurthy and Reddy.

TABLE IV. Comparison of temperature coefficients of the second-order elastic constants of calcite (in units of 10^{-4}/°C).

	Present work[a] at 0°C	Reddy and Subrahmanyam[b]	Ramamurthy and Reddy[c]
$\partial \ln c_{11}/\partial T$	−3.898	15.5	89.3
$\partial \ln c_{12}/\partial T$	−5.273	48.4	−175.8
$\partial \ln c_{13}/\partial T$	−4.825	36.8	138.8
$\partial \ln c_{14}/\partial T$	−2.838	9.79	−38.01
$\partial \ln c_{33}/\partial T$	−1.462	16.7	89.87
$\partial \ln c_{44}/\partial T$	−2.753	3.46	28.37

[a] The linear thermal-expansion coefficients α in Table I, and the volume thermal-expansion coefficient γ of Rosenholtz *et al.* ($\approx 13.14\times10^{-6}$/°C) (Ref. 58), were used in Eq. (31).
[b] Average values between 0 and 200°C, Ref. 60.
[c] Average values between 0 and 30°C, Ref. 61.

TABLE V. Third-order elastic constants of calcite at 0°C (in units of 10^{12} dyn/cm^2).[a]

C_{111}	−5.79±0.17	C_{134}	0.82±0.05
C_{112}	−1.47±0.14	C_{144}	−0.69±0.12
C_{113}	−1.93±0.06	C_{155}	−1.39±0.07
C_{114}	2.18±0.15	C_{222}	−6.75±0.19
C_{123}	−0.41±0.12	C_{333}	−4.98±0.13
C_{124}	0.10±0.06	C_{344}	−1.95±0.06
C_{133}	−2.39±0.11	C_{444}	0.33±0.10

[a] Cases $4A$ and $8H$ were not taken into account in this best-fit evaluation.

Computation of the third-order elastic constants has been carried out from the data in Figs. 5 and 6 using the expressions [Eqs. (14) and (15)] for $-[\partial(\rho_0 W^2)/\partial p]_{p=0}$ similar to those used by Thurston *et al.*[30] For 24 cases (modes 1–8) the expressions were equivalent to theirs, but for the other nine cases (modes 10–12) independent expressions were expanded from Eqs. (14) and (15). Eleven hydrostatic measurements can give only six independent relations corresponding to the pressure derivatives of the six second-order constants. Twenty-two uniaxial measurements were sufficient to determine 14 third-order constants of calcite with crosschecks. Nevertheless eleven hydrostatic-pressure runs were made to furnish additional crosschecks. Fourteen third-order elastic constants of calcite at 0°C were thus determined with a least-squares best fit. Out of the 33 independent cases, large uncertainties were involved in the determi-

TABLE VI. Pressure derivatives of the thermodynamic and the conventional second-order elastic constants of calcite at 0°C.

B_{11}[a]	3.59	$\partial c_{11}/\partial p$	3.02
B_{12}	0.88	$\partial c_{12}/\partial p$	2.05
B_{13}	2.64	$\partial c_{13}/\partial p$	3.19
B_{14}	−1.31	$\partial c_{14}/\partial p$	−1.25
B_{33}	5.47	$\partial c_{33}/\partial p$	2.80
B_{44}	2.20	$\partial c_{44}/\partial p$	0.92
B_{66}[b]	1.35	$\partial c_{66}/\partial p$[b]	0.49

[a] $B_{\lambda\mu}(B_{ijkl})$ are the thermodynamic pressure derivatives defined as $[\partial(\partial^2\Phi/\partial\eta_{ij}\partial\eta_{kl})/\partial p]_T$.
[b] B_{66} and $\partial c_{66}/\partial p$ are not independent derivatives.

[60] P. J. Reddy and S. V. Sabrahmanyam, Acta Cryst. 13, 493 (1960).
[61] L. Ramamurthy and P. J. Reddy, J. Phys. Chem. Solids 28, 2131 (1967).

TABLE VII. Temperature dependence of linear combinations of the third-order elastic constants of calcite at 0°C (in units of 10^{-2}/°C).

Symbols	Expression for B_{ij}	$\left[\frac{1}{B_{ij}}\frac{\partial B_{ij}}{\partial T}\right]$
B_{11}	$-s_1(C_{111}+C_{112})-s_3C_{113}$	4.81
B_{12}	$-s_1(C_{111}+2C_{112}-C_{222})-s_3C_{123}$	3.77
B_{13}	$-s_1(C_{113}+C_{123})-s_3C_{133}$	17.12
B_{14}	$-s_1(C_{114}+C_{124})-s_3C_{134}$	10.22
B_{33}	$-2s_1C_{133}-s_3C_{333}$	2.24
B_{44}	$-s_1(C_{144}+C_{155})-s_3C_{344}$	6.09
B_{66}[a]	$-\frac{1}{2}[s_1(C_{222}-C_{112})-s_3(C_{113}-C_{123})]$[a]	0.84

[a] This is not an independent expression.

TABLE VIII. Comparison of the isothermal-bulk moduli and their pressure derivatives at room temperature.

	Present work	Bridgman[a]
B^T(isothermal)	7.156×10^{11} dyn/cm^2	7.315×10^{11} dyn[b]/cm^2
$\left[\frac{\partial B}{\partial p}\right]_{p=0}$	4.828[c]	4.174[b]

[a] Reference 63.
[b] These were calculated as $1/A_1$ and $2A_2/A_1^2$, respectively, for B^T and $[\partial B/\partial p]_{p=0}$ from measurements of the change in compressibility with pressure $-\Delta v/v_0=A_1p-A_2p^2$.
[c] The pressure derivative of the adiabatic bulk modulus at 0°C. The pressure derivative of the isothermal bulk modulus at room temperature in this case is different only by 1–2%.

nation of $(1/W)(\Delta W/p)$ for cases $4A$ and $8H$, so these were not taken into account in the best fit. No weighting of the data was used because this gave minimum standard deviations compared with other weighting schemes. The hydrostatic measurements were not necessarily more reliable than the uniaxial ones in the determination of $(1/W)(\Delta W/p)$, although the over-all change in $\Delta W/p$ was relatively larger. The best-fit third-order constants are tabulated in Table V. The relatively large probable errors seem to result because the stress range was limited (one order of magnitude smaller than for quartz), and because many coefficients had to be simultaneously fitted.

The pressure derivatives of the thermodynamic second-order elastic constants $B_{ij}(B_{prqs})$ defined by $[\partial(\partial^2\Phi/\partial\eta_i\partial\eta_j)_S/\partial p]_T$ or by Eq. (14),[30,62] are convenient physical quantities. Compared with third-order constants, they are directly connected to changes in the natural velocities with hydrostatic pressure, and a relatively small number of them (six for a trigonal crystal) gives full information about such first-order anharmonic properties as the conventional pressure derivatives of the second-order elastic constants $\partial c_{ij}/\partial p$, and the change in compressibility with pressure. In Table VI the six B_{ij}'s were evaluated from the set of third-order constants of Table V using the relation

$$B_{ij}=[(\partial/\partial p)(\partial^2\Phi/\partial\eta_i\partial\eta_j)]_T = -s_1(C_{1ij}+C_{2ij})-s_3C_{3ij}, \quad (32)$$

where $s_1=s_{11}{}^T+s_{12}{}^T+s_{13}{}^T$ and $s_3=2s_{13}{}^T+s_{33}{}^T$. The conventional pressure derivatives of the second-order constants $\partial c_{ij}/\partial p$ can also be computed from B_{ij} or linear combinations of third-order constants as follows: The true sound velocity in the specimen under pressure is expressed (using the fractional change in volume γ_p, and the longitudinal strain α_p in the propagation direction caused by pressure p) as

$$\rho V^2=\frac{\rho_0}{1+\gamma_p}\left\{\frac{d_s(1+\alpha_p)}{\tau}\right\}^2=\rho_0W^2\frac{(1+\alpha_p)^2}{1+\gamma_p}, \quad (33)$$

where ρ and ρ_0 are the density of the specimen, respectively, under pressure p and zero pressure; d_s is twice

TABLE IX. Rhombohedral angle θ; lattice constants a, d; repulsive force law exponents n_{11}, n_{12}, n_{22}; and force constants μ_{11}, μ_{12}, μ_{22} of calcite-type crystals[a] ($n_{22}=11$, $\mu_{22}=17.6\times10^{-88}$ erg cm^{10}, and the distance b is 1.08 Å for the carbonates and 0.70 Å for $NaNO_3$).

	θ(obs.)	a and d[b](Å)	n_{11} and μ_{11}(erg cm$^{n_{11}-1}$)	n_{12} and μ_{12}(erg cm$^{n_{12}-1}$)	
$CaCO_3$	101°55′	4.99[c]	9	10	
		1.417	2.45×10^{-7}	2.07×10^{-80}	
$CdCO_3$	102°30′	4.92	···	10	11
		1.371	···	1.76×10^{-80}	4.40×10^{-80}
$MnCO_3$	102°50′	4.77	···	10	11
		1.3132	···	1.00×10^{-80}	2.40×10^{-88}
$\frac{1}{2}(MgCa)CO_3$	102°53′	4.78	10	10	11
		1.3127	0.176×10^{-80}	1.05×10^{-80}	2.50×10^{-88}
$FeCO_3$	103°4.5′	4.70	···	10	11
		1.282	···	0.77×10^{-80}	1.71×10^{-88}
$ZnCO_3$	103°28′	4.64	···	10	11
		1.247	···	0.62×10^{-80}	1.43×10^{-88}
$MgCO_3$	103°21.5′	4.61	11	···	11
		1.244	5.84×10^{-90}	···	1.51×10^{-88}
$NaNO_3$	102°42.5′	5.070[d]	11	···	11
		1.402	0.232×10^{-88}	···	2.55×10^{-88}

[a] θ and a were taken from S. Chapman, J. Topping, and J. Morrall, Proc. Roy. Soc. **111**, 25 (1926) except for $CaCO_3$ and $NaNO_3$, and the force-law exponents and force constants from Refs. 65, 66, and 67.
[b] d was calculated from $d=a[1/(4\sin^2\theta/2)-\frac{1}{3}]^{1/2}$.
[c] H. Chessin and W. C. Hamilton, Acta Cryst. **18**, 689 (1965).
[d] H. E. Swanson, N. T. Gilfrick, and M. I. Cook, Natl. Bur. Std. (U. S.) Circ. **539**, 50 (1956).

[62] R. N. Thurston, J. Acoust. Soc. Am. **37**, 348 (1965).

the specimen thickness in the propagation direction, and τ is the round-trip delay time. Since the crystal symmetry is conserved, the derivative of Eq. (33) with respect to p is given as

$$[\rho V^2]'_{p=0}=[\rho_0 W^2]'_{p=0}+(\rho_0 W^2)_{p=0} \times[2(\partial\alpha_p/\partial p)_{p=0}+2s_1+s_3], \quad (34)$$

or using Eq. (14) for $[\rho_0 W^2]'_{p=0}$ and $w=(\rho_0 W^2)_{p=0}$,

$$[\rho V^2]'_{p=0}=-G_{\rm HC}-1 +w(2s_1+s_3+2(\partial\alpha_p/\partial p)_{p=0}-2F_{\rm HC}). \quad (35)$$

In Eq. (35) the left-hand side is directly related to $\partial c_{ij}/\partial p$ evaluated at $p=0$. If, for example, the propagation direction is along one of the three axes (X,Y,Z) in calcite, the pressure derivative of the principal strain $(\partial\alpha_{p,ii}/\partial p)$ $(i=1, 2, 3)$ is given by

$$(\partial\alpha_{p,ii}/\partial p)_{p=0}=-s_i, \quad (36)$$

with $s_2=s_3$ for a trigonal crystal. From Eqs. (35) and (36), $(\partial c_{11}/\partial p)_{p=0}$ is therefore calculated as

$$(\partial c_{11}/\partial p)_{p=0}=B_{11}-1+(s_3-2s_1)c_{11}. \quad (37)$$

A set of $(\partial c_{ij}/\partial p)_{p=0}$ for calcite calculated from Eq. (35) with the third-order elastic constants is included in Table VI. The pressure derivatives of the second-order elastic constants B_{ij} and $\partial c_{ij}/\partial p$ are all positive except for B_{14} and $\partial c_{14}/\partial p$, which are negative.

It was noticed that the temperature coefficients of the natural velocities under pressure were significantly different from those at zero pressure. Since $\rho_0 W^2$ at pressure p is experimentally given by

$$\rho_0 W^2=w+p(-1-2wF_{\rm HC}-G_{\rm HC}), \quad (38)$$

the main difference seems to arise from the contribution of the second term; that is, from the change in the pressure coefficient with temperature. Hence, one can calculate the temperature dependence of the second term (which is, of course, proportional to p), and compare it with that of the first term. Under a hydrostatic pressure of about 100 kg/cm^2, the second-term contribution amounted to 20 to 40% of the total effective temperature dependence for modes 10 and 11. It was a little less than 10%, but definitely larger than the experimental errors, for the other modes. Furthermore, the temperature dependences of the thermodynamic-pressure derivatives $\partial B_{ij}/\partial T$ were calculated and are given in Table VII. All the coefficients $(1/B_{ij})(\partial B_{ij}/\partial T)$ are positive and much larger than the coefficients $(1/c_{ij}) \times(\partial c_{ij}/\partial T)$.

Except for the temperature dependences of the second-order constants[60,61] and some pressure measurements by Bridgman,[63] there have been no data reported on the anharmonicity of calcite for comparison with the present results. Bridgman[63] fitted changes in the compressibility of calcite by a quadratic expression $-\Delta v/v_0 =A_1 p-A_2 p^2$, where Δv is the change in volume from the initial volume v_0 at zero pressure, to the pressure p, and A_1 and A_2 are the constants obtained by this fit. In order to compare the third-order constants of Table V with Bridgman's results, the pressure derivative $(\partial B/\partial p)_{p=0}$ of the effective bulk modulus B was calculated from both measurements. In Bridgman's notation it is $2A_2/A_1^2$, whereas in the present notation

$$(\partial B/\partial p)_{p=0}=-2B^2\{(1/B)+(1/\beta^2)\{\beta[B_{11}+B_{12}-4B_{13}+2B_{33} -6+(s_3-2s_1)(c_{11}+c_{12})+2(2s_1-3s_3)c_{33}+4s_3c_{13}]-(c_{11}+c_{12}-4c_{13}+2c_{33})[[B_{33}-1+(2s_1-3s_3)c_{33}] \times(c_{11}+c_{12})+c_{33}[B_{11}+B_{12}+(s_3-2s_1)(c_{11}+c_{12})]-4c_{13}(B_{13}+1-s_3c_{13})]\}\}, \quad (39)$$

where $B=1/(2s_1+s_3)$ and $\beta=c_{33}(c_{11}+c_{12})-2c_{13}^2$. Values of both $(\partial B/\partial p)_{p=0}$ and the isothermal bulk modulus B^T are compared with those of Bridgman in Table VIII. The agreement between the two $(\partial B/\partial p)_{p=0}$ values is good. Therefore, a reasonable set of third-order elastic constants for calcite has been obtained in the present work.

V. DISCUSSION

For alkali-halide crystals the contribution from the closed ion-core repulsive interactions to the third-order elastic constants is predominant as compared with other factors.[9–12] Therefore, it is of some interest to calculate this contribution $C_{ijk}{}^R$ to the third-order constants and compare it with experiment. Although a substantial contribution may come also from the electrostatic interactions,[9–12] attention will be confined here to the former contribution (the exact evaluation of the electrostatic contribution is a more complicated problem because of the nature of the long-range force). The isomorphous series of carbonate crystals of the calcite type (including one nitrate crystal) $CaCO_3$, $CdCO_3$, $MnCO_3$, $\frac{1}{2}(MgCa)CO_3$, $FeCO_3$, $ZnCO_3$, $MgCO_3$, $NaNO_3$ will be considered.

In the calcite structure there are six different ion-pair types, but the carbon (or nitrogen) atoms are deeply buried inside oxygen triads so the carbon atoms will not be considered explicitly and the number of different ion pairs is reduced to three: metal-ion–metal-ion (M-M), metal-ion–oxygen-ion (M-O), and oxygen-ion–oxygen-ion (O-O).

To describe the repulsive potentials $\phi^R(r)$, inverse power functions may be used.[1,64] If r is the ion-separa-

[63] P. W. Bridgman, Am. J. Sci. **10**, 483 (1925).

tion distance, they are given by

$$\phi^R(r)=[\mu/(n-1)](1/r^{n-1}) \tag{40}$$

with the force constants μ and the force-law exponents n given by Lennard-Jones and Dent.[65-68]

We denote the repulsive potential, its exponent, and its force constant for the M-M ion pair by $\phi_{11}{}^R(r)$, n_{11}, and μ_{11}; those for the M-O ion pair by $\phi_{12}{}^R(r)$, n_{12}, and μ_{12}; and those for the O-O ion pair by $\phi_{22}{}^R(r)$, n_{22}, and μ_{22}. In Table IX, these constants are tabulated for eight calcite-type crystals.

Let us first calculate the repulsive contributions $C_{ijk}{}^R$ to the third-order elastic constants for $CaCO_3$, $\frac{1}{2}$(MgCa)-CO_3, $MgCO_3$, and $NaNO_3$. The cleavage unit cell of calcite has been shown in Fig. 1, and Fig. 7 presents its projection along the trigonal axis onto the xy plane where the CO_3 groups are in a hexagonal array. The rhombohedral angle θ and the structural distances a, d, and b are indicated in one of these figures. The distance between two calcium atoms or two CO_3 groups is a, the distance between two neighboring atomic layers of calcium and CO_3 groups along the trigonal axis is d, and the distance between the repulsive force centers of the carbon and oxygen atoms of the same CO_3 group is b. The same approach used by Lennard-Jones and Dent[66] to calculate the repulsive potential energy of one molecule is followed. The total repulsive contribution $C_{ijk}{}^R$ is divided into three contributions: the interaction between one M ion and all the other M ions $C_{ijk}{}^{R,\text{M-M}}$; the interaction between one M ion and all the CO_3 groups $C_{ijk}{}^{R,\text{M-CO}_3}$ (or the inverse, $C_{ijk}{}^{R,\text{CO}_3\text{-M}}$); and the interaction between one CO_3 group and the rest $C_{ijk}{}^{R,\text{CO}_3\text{-CO}_3}$. Thus,

$$C_{ijk}{}^R=C_{ijk}{}^{R,\text{M-M}}+2C_{ijk}{}^{R,\text{M-CO}_3}+C_{ijk}{}^{R,\text{CO}_3\text{-CO}_3}, \tag{41}$$

where the factor 2 in the second term arises from the fact that there are two equal contributions, $C_{ijk}{}^{R,\text{M-CO}_3}$ and $C_{ijk}{}^{R,\text{CO}_3\text{-M}}$ for one molecule. In calculating these terms, contributions up to the next-nearest group interactions are included. If the coordinates of ions at (a_1,a_2,a_3) are denoted by (l_1,l_2,l_3) with respective unit lengths $\frac{1}{2}a$, $\frac{1}{2}\sqrt{3}a$, and d, as in Fig. 7; and the third derivatives of the repulsive potential are denoted by $u_{ij}{}^R(r)\equiv D^3\phi_{ij}{}^R(r)=-\mu_{ij}(n_{ij}+1)(n_{ij}+3)/r^{n_{ij}+5}$; then the repulsive contribution [Eq. (41)] to each third-order elastic constant can be explicitly written down from Eq. (9):

$$C_{111}{}^R=(2V_c)^{-1}(\tfrac{1}{2}a)^6\{\sum_{\text{M-M}} l_1{}^6u_{11}(r)+2\sum_{\text{M-CO}_3} l_1{}^6u_{12}(r)+\sum_{\text{CO}_3\text{-CO}_3} l_1{}^6u_{22}(r)\},$$

$$C_{112}{}^R=(2V_c)^{-1}(\tfrac{1}{2}a)^4(\tfrac{1}{2}\sqrt{3}a)^2\{\sum_{\text{M-M}} l_1{}^4l_2{}^2u_{11}(r)+2\sum_{\text{M-CO}_3} l_1{}^4l_2{}^2u_{12}(r)+\sum_{\text{CO}_3\text{-CO}_3} l_1{}^4l_2{}^2u_{22}(r)\},$$

$$C_{113}{}^R=C_{155}{}^R=(2V_c)^{-1}(\tfrac{1}{2}a)^4d^2\times\{\sum_{\text{M-M}} l_1{}^4l_3{}^2u_{11}(r)+2\sum_{\text{M-CO}_3} l_1{}^4l_3{}^2u_{12}(r)+\sum_{\text{CO}_3\text{-CO}_3} l_1{}^4l_3{}^2u_{22}(r)\},$$

$$C_{114}{}^R=(2V_c)^{-1}(\tfrac{1}{2}a)^4(\tfrac{1}{2}\sqrt{3}a)d\times\{\sum_{\text{M-M}} l_1{}^4l_2l_3u_{11}(r)+2\sum_{\text{M-CO}_3} l_1{}^4l_2l_3u_{12}(r)+\sum_{\text{CO}_3\text{-CO}_3} l_1{}^4l_2l_3u_{22}(r)\},$$

$$C_{123}{}^R=C_{144}{}^R=(2V_c)^{-1}(\tfrac{1}{2}a)^2(\tfrac{1}{2}\sqrt{3}a)^2d^2\times\{\sum_{\text{M-M}} l_1{}^2l_2{}^2l_3{}^2u_{11}(r)+2\sum_{\text{M-CO}_3} l_1{}^2l_2{}^2l_3{}^2u_{12}(r)+\sum_{\text{CO}_3\text{-CO}_3} l_1{}^2l_2{}^2l_3{}^2u_{22}(r)\},$$

$$C_{124}{}^R=(2V_c)^{-1}(\tfrac{1}{2}a)^2(\tfrac{1}{2}\sqrt{3}a)^3d\times\{\sum_{\text{M-M}} l_1{}^2l_2{}^3l_3u_{11}(r)+2\sum_{\text{M-CO}_3} l_1{}^2l_2{}^3l_3u_{12}(r)+\sum_{\text{CO}_3\text{-CO}_3} l_1{}^2l_2{}^3l_3u_{22}(r)\}, \tag{42}$$

$$C_{133}{}^R=C_{344}{}^R=(2V_c)^{-1}(\tfrac{1}{2}a)^2d^4\times\{\sum_{\text{M-M}} l_1{}^2l_3{}^4u_{11}(r)+2\sum_{\text{M-CO}_3} l_1{}^2l_3{}^4u_{12}(r)+\sum_{\text{CO}_3\text{-CO}_3} l_1{}^2l_3{}^4u_{22}(r)\},$$

$$-C_{134}{}^R=C_{444}{}^R=(2V_c)^{-1}(\tfrac{1}{2}\sqrt{3}a)^3d^3\times\{\sum_{\text{M-M}} l_2{}^3l_3{}^3u_{11}(r)+2\sum_{\text{M-CO}_3} l_2{}^3l_3{}^3u_{12}(r)+\sum_{\text{CO}_3\text{-CO}_3} l_2{}^3l_3{}^3u_{22}(r)\},$$

$$C_{222}{}^R=(2V_c)^{-1}(\tfrac{1}{2}\sqrt{3}a)^6\{\sum_{\text{M-M}} l_2{}^6u_{11}(r)+2\sum_{\text{M-CO}_3} l_2{}^6u_{12}(r)+\sum_{\text{CO}_3\text{-CO}_3} l_2{}^6u_{22}(r)\},$$

$$C_{333}{}^R=(2V_c)^{-1}d^6\{\sum_{\text{M-M}} l_3{}^6u_{11}(r)+2\sum_{\text{M-CO}_3} l_3{}^6u_{12}(r)+\sum_{\text{CO}_3\text{-CO}_3} l_3{}^6u_{22}(r)\},$$

[64] M. Born and K. Huang, *Dynamical Theory of Crystal Lattices* (Oxford University Press, Oxford, 1954), p. 19.
[65] J. E. Lennard-Jones and B. M. Dent, Proc. Roy. Soc. (London) **112**, 230 (1926).
[66] J. E. Lennard-Jones and B. M. Dent, Proc. Roy. Soc. (London) **113**, 673 (1927).
[67] J. E. Lennard-Jones and B. M. Dent, Proc. Roy. Soc. (London) **113**, 690 (1927).
[68] J. E. Lennard-Jones, Proc. Roy. Soc. (London) **A109**, 584 (1925).

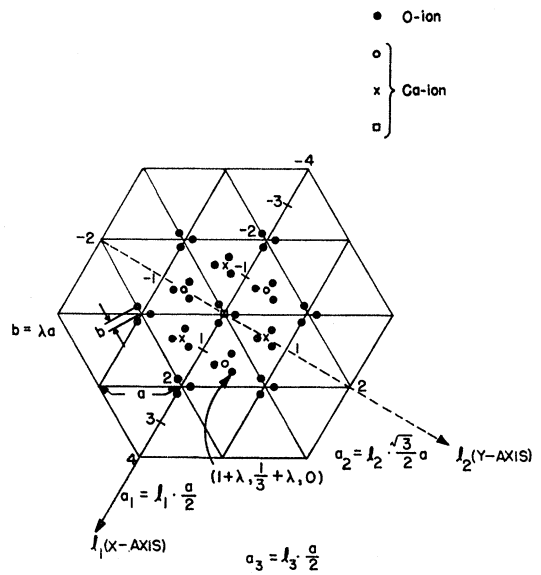

FIG. 7. Projection onto a CO_3 plane normal to the trigonal axis of calcite. All of the ions in the cleavage unit cell of Fig. 1 that were considered in the calculation of the text are shown. C ions are not shown for clearness. Solid circles (●) clustered in groups of three near the intersections of the solid lines denote oxygen atoms lying in the CO_3 projection plane; open circles (○) and crosses (×) denote calcium atoms, one atomic layer below and above it, respectively; solid circles around the calcium atoms denote oxygen atoms two layers above and below it; and the square at the center of the hexagon denotes two calcium atoms three layers above and below it.

where $u_{ij}(r) \equiv u_{ij}{}^R(r_{\mu\nu})$ is understood, and the unit cell volume is $V_c = 2r_0{}^3 \sin^2\theta$, where r_0 is the nearest-neighbor distance between the centers of an M ion and a CO_3 group, being given by $a/2 \sin\theta$. The summations in Eq. (42) are to be taken over the ion pairs at nearest and next-nearest groups, i.e., only for the ions shown in Fig. 7. Numerical results for the individual terms $C_{ijk}{}^{R,\text{M-M}}$, $2C_{ijk}{}^{R,\text{M-CO}_3}$, $C_{ijk}{}^{R,\text{CO}_3\text{-CO}_3}$ are shown in Table X for $CaCO_3$ and $MgCO_3$. (Results for $\frac{1}{2}$(MgCa)CO_3 and $NaNO_3$ are given in Table XI only for the total contributions $C_{ijk}{}^R$.)

In Table X, $C_{ijk}{}^{R,\text{M-M}}$ is very small in magnitude in comparison with the other terms, being less than 1% of the total $C_{ijk}{}^R$. Thus, by neglecting the first term in Eq. (41) the total repulsive contributions $C_{ijk}{}^R$ for $CdCO_3$, $MnCO_3$, $FeCO_3$, and $ZnCO_3$ have been obtained and are given in the second row of each crystal in Table XI. (In this table only the data for $n_{12}=10$ in the case of $CdCO_3$ and $n_{12}=11$ in the case of $MnCO_3$, $\frac{1}{2}$(MgCa)CO_3, $FeCO_3$, $ZnCO_3$ are presented.)

Some qualitative properties of the third-order elastic constants of calcite can be pointed out. In Table V two constants (C_{114} and C_{134}) among 14 are definitely positive; the others are negative or nearly zero. This differs from α-quartz, where all 14 constants are negative or nearly zero.[30] Calcite has nearly equal, large negative values for C_{111}, C_{222}, and C_{333}, intermediate values for C_{112}, C_{113}, C_{114}, C_{133}, C_{155}, and C_{344}, and almost vanishing values for C_{123}, C_{124}, C_{134}, C_{144}, and C_{444}. It may be seen

TABLE X. Contributions of the various terms in the repulsive interaction Eq. (41) for $CaCO_3$ and $MgCO_3$ (in units of 10^{12} dyn/cm^2).

Crystals	n_{12} b (Å)	Contributing terms	$C_{111}{}^R$	$C_{112}{}^R$	$C_{113}{}^R$	$C_{114}{}^R$	$C_{123}{}^R$	$C_{124}{}^R$	$C_{133}{}^R$	$C_{134}{}^R$	$C_{144}{}^R$	$C_{155}{}^R$	$C_{222}{}^R$	$C_{333}{}^R$	$C_{344}{}^R$	$C_{444}{}^R$
$CaCO_3$	$b=1.08$[a] $n_{12}=10$	$C_{ijk}{}^{R,\text{Ca-Ca}}$	−0.020	−0.004	−0.009	−0.005	−0.003	−0.002	−0.012	−0.006			−0.019	−0.024		
		$2C_{ijk}{}^{R,\text{Ca-CO}_3}$	−8.86	−1.68	−4.83	2.40	−1.61	0.799	−3.09	1.51	$C_{123}{}^R$	$C_{113}{}^R$	−8.71	−3.38	$C_{133}{}^R$	$-C_{134}{}^R$
		$C_{ijk}{}^{R,\text{CO}_3\text{-CO}_3}$	−3.69	−0.741	−0.603	−0.0748	−0.201	−0.0249	−1.75	−0.0608			−3.68	−9.42		
		$C_{ijk}{}^R$	−12.57	−2.43	−5.45	2.32	−1.82	0.77	−4.86	1.45			−12.40	−12.82		
$MgCO_3$	$b=1.08$[a] $n_{12}=11$	$C_{ijk}{}^{R,\text{Mg-Mg}}$	−0.0011	−0.0003	−0.0007	−0.0004	−0.0002	−0.0001	−0.0009	−0.0005			−0.0012	−0.0015		
		$2C_{ijk}{}^{R,\text{Mg-CO}_3}$	−13.01	−2.20	−6.93	3.11	−2.31	1.03	−4.32	1.93	$C_{123}{}^R$	$C_{113}{}^R$	−12.35	−4.37	$C_{133}{}^R$	$-C_{134}{}^R$
		$C_{ijk}{}^{R,\text{CO}_3\text{-CO}_3}$	−14.37	−3.19	−2.71	−0.213	−0.903	−0.0711	−7.85	0.0848			−14.82	−40.79		
		$C_{ijk}{}^R$	−27.38	−5.39	−9.64	2.90	−3.21	0.97	−12.18	2.01			−27.17	−45.16		

[a] This was obtained theoretically by Lennard-Jones and Dent in Ref. 66 for the distance between the two repulsive force centers of a carbon ion and an oxygen ion of the same CO_3 group.

TABLE XI. Semiempirical estimation of the third-order elastic constants for some carbonate crystals of the calcite type (in units of 10^{12} dyn/cm^2).[a]

Crystals	C_{111}	C_{112}	C_{113}	C_{114}	C_{123}	C_{124}	C_{133}	C_{134}	C_{144}	C_{155}	C_{222}	C_{333}	C_{344}	C_{444}
	6.78	0.96	3.52	−0.14	1.41	−0.67	2.47	−0.63	1.13	4.06	5.65	7.84	2.91	1.78
	−12.57	−2.43	−5.45	2.32	−1.82	0.77	−4.86	1.45	−1.82	−5.45	−12.40	−12.82	−4.86	−1.45
$CaCO_3$	−5.79	−1.47	−1.93	2.18	−0.41	0.10	−2.39	0.82	−0.69	−1.39	−6.75	−4.98	−1.95	0.33
	7.22	1.02	3.72	−0.15	1.49	−0.71	2.61	−0.67	1.20	4.30	5.98	8.30	3.08	1.88
	−14.89	−2.86	−6.24	2.55	−2.08	0.85	−5.84	1.58	−2.08	−6.24	−14.66	−16.69	−5.84	−1.58
$CdCO_3$	−7.67	−1.84	−2.52	2.40	−0.59	0.14	−3.23	0.91	−0.88	−1.94	−8.68	−8.39	−2.76	0.30
	8.17	1.15	4.22	−0.17	1.69	−0.80	2.96	−0.75	1.35	4.86	6.77	9.39	3.49	2.13
	−19.08	−3.68	−7.43	2.68	−2.48	0.89	−7.96	1.73	−2.48	−7.43	−18.80	−25.93	−7.96	−1.73
$MnCO_3$	−10.91	−2.53	−3.21	2.51	−0.79	0.09	−5.00	0.98	−1.13	−2.57	−12.03	−16.53	− 4.47	0.40
	8.10	1.14	4.18	−0.17	1.67	−0.80	2.93	−0.75	1.34	4.82	6.71	9.31	3.46	2.11
	−19.11	−3.68	−7.53	2.74	−2.51	0.91	−7.96	1.75	−2.51	−7.53	−18.83	−25.65	−7.96	−1.75
$\frac{1}{2}(MgCa)CO_3$	−11.01	−2.54	−3.35	−2.57	−0.84	0.11	−5.03	1.00	−1.17	−2.71	−12.12	−16.34	−4.50	0.36
	8.67	1.22	4.48	−0.18	1.79	−0.85	3.14	−0.80	1.44	5.16	7.18	9.96	3.70	3.26
	−20.69	−4.05	−7.47	2.40	−2.49	0.80	−9.01	1.60	−2.49	−7.47	−20.48	−32.47	−9.01	−1.60
$FeCo_3$	−12.02	−2.83	−3.00	2.22	−0.70	−0.05	−5.87	0.80	−1.05	−2.31	−13.30	−22.51	−5.31	0.66
	9.12	1.28	4.71	−0.19	1.89	−0.90	3.30	−0.84	1.51	5.43	7.56	10.49	3.89	2.38
	−24.48	−4.82	−8.61	2.54	−2.87	0.85	−11.13	1.75	−2.87	−8.61	−24.29	−41.93	−11.13	−1.75
$ZnCO_3$	−15.36	−3.54	−3.90	2.35	−0.98	−0.05	−7.83	0.91	−1.36	−3.18	−16.73	−31.44	−7.24	0.63
	9.36	1.32	4.83	−0.19	1.94	−0.92	3.39	−0.86	1.55	5.57	7.76	10.76	3.99	2.44
	−27.38	−5.39	−9.64	2.90	−3.21	0.97	−12.18	2.01	−3.21	−9.64	−27.17	−45.16	−12.18	−2.01
$MgCO_3$	−18.02	−4.07	−4.81	2.71	−1.27	0.05	−8.79	1.15	−1.66	−4.07	−19.41	−34.40	−8.19	0.43
$NaNO_3$[b] C_{ijk}^R	−3.84	−0.89	−1.64	0.61	−0.55	0.20	−1.66	−0.04	−0.55	−1.64	−4.01	−4.60	−1.66	−0.04

[a] The first row for each crystal is C_{ijk}^e, the second row is C_{ijk}^R, and the third row is the total third-order elastic constant C_{ijk}.
[b] C_{ijk}^e and C_{ijk} were not estimated for $NaNO_3$.

in Table X that these differences in magnitude stem mainly from the differences in the repulsive contributions C_{ijk}^R. One interesting point is that the signs of the measured constants C_{ijk} coincide with the signs of C_{ijk}^R except for C_{444} whose value is small and comparable with the experimental error. It seems, therefore, that the contribution from the short-range repulsive interaction plays an important role in determining the C_{ijk} of calcite just as in the alkali halides[9–15] and the noble metals.[28]

The relative importance of the various terms in Eq. (41) can be found from Table X. In calcite the second term $2C_{ijk}^{R,\text{Ca-CO}_3}$ has the largest contributions, the third term $C_{ijk}^{R,\text{CO}_3\text{-CO}_3}$ the next largest contributions, and the first term $C_{ijk}^{R,\text{Ca-Ca}}$ the negligibly small contributions to all C_{ijk}^R except for C_{333}^R, where the relative weights of $2C_{ijk}^{R,\text{Ca-CO}_3}$ and $C_{ijk}^{R,\text{CO}_3\text{-CO}_3}$ are reversed. In passing from $CaCO_3$ towards $MgCO_3$, the relative importance of the third term is emphasized more and more with a decrease in the lattice constants, and in $MgCO_3$ the third term is larger than the second term for C_{111}^R, C_{112}^R, C_{133}^R, C_{222}^R, C_{333}^R, and C_{344}^R. For $CaCO_3$, $C_{111}^R \approx C_{222}^R \approx C_{333}^R$, and as we go towards $MgCO_3$, this relation begins to break down and C_{333}^R surpasses the other two, but the approximate equality $C_{111}^R \approx C_{222}^R$ holds for all the carbonates and $NaNO_3$ (Table XI). Therefore, the compressional elastic constants C_{iii} ($i=1, 2$) of all the carbonates is nearly isotropic in two directions (X and Y) at least up to the third order, that is, approximately isotropic in the xy plane. This interestingly corresponds to the isotropic linear thermal expansion coefficient in this plane (Table I).

Calcite has three negative pressure coefficients of the natural velocity, $(1/W)\Delta W/p$ for modes $3H$, $11H$, and $12H$ (Fig. 6). As to the pressure dependence of the true velocity $\partial(\rho V^2)/\partial p$, only two coefficients $(\partial/\partial p)(c_{66}+c_{14}\times\tan\nu)$ for $3H$, ($\tan\nu=1.34813$) and $(\partial/\partial p)[\frac{1}{2}(c_{66}+c_{44}+2c_{14})]$ for $12H$, are negative. These negative coefficients are due to the fairly large negative $\partial c_{14}/\partial p$ and hence, to the positive third-order constants C_{114}, C_{124}, C_{134} (especially to large C_{114}) through the expression $\partial c_{14}/\partial p = -s_1 c_{14} - s_1(C_{114}+C_{124}) - s_3 C_{134}$. The negative pressure dependence for calcite-type crystals is of some interest, being analogous to the negative $\partial c_{44}/\partial p$ of some NaCl-type crystals with large ionic radii.[11,69]

[69] K. M. Koliwad, P. B. Ghate, and A. L. Ruoff, Phys. Status Solidi 21, 507 (1967).

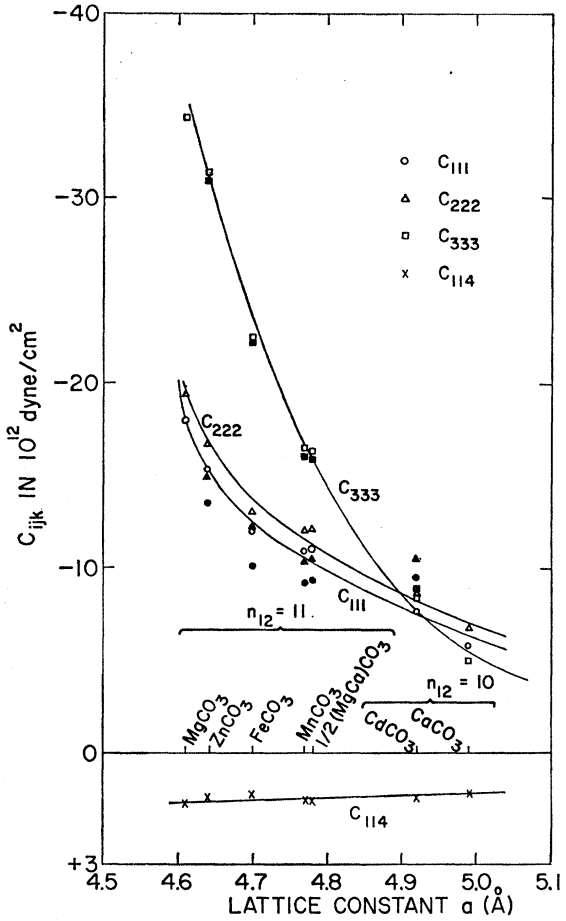

FIG. 8. Variation of the third-order elastic constants with lattice constant a for the isomorphous series of the calcite-type crystals (open symbols and crosses). The solid symbols are additional data associated with $n_{12}=11$ for $CdCO_3$, $n_{12}=10$ for $MnCO_3$, $\frac{1}{2}(MgCa)CO_3$, $FeCO_3$, $ZnCO_3$.

Now let us examine the Cauchy relations which are commonly used to test the nonionic nature of binding forces in ionic crystals.[2–5] Calcite is composed of Ca ions and CO_3 groups, where the CO_3 radicals are tightly bound within themselves by the formation of a planar triad of electron-pair bonds,[39] i.e., covalent bonds, as in the tetrahedral bonds of CH_4 or diamond-like crystals. However, since this covalent nature does not come into play, the elastic properties of calcite may depend only on the bond characters between Ca ion and Ca ion, Ca ion and CO_3 radical, and CO_3 radical and CO_3 radical. The CO_3 triads do not have spherical symmetry so noncentral forces must act between them, and this should be reflected in deviations from the Cauchy equalities. The Cauchy relations for a trigonal crystal are given by Eqs. (10) and (11), and the experimental values are arranged in Table XII to make it easy to see their deviations. Also shown in parentheses in Table XII are experimental data obtained by Thurston *et al.*[30] for α-quartz (a comparative trigonal crystal). The Cauchy

TABLE XII. Test of the Cauchy relations for the second-(10^{11}dyn/cm^2) and the third-order elastic constants (10^{12}dyn/cm^2) in calcite and α quartz (in parentheses).[a]

Symbols[b]	Corresponding numerical values[b]
c_{13}/c_{44}	5.280 / 3.289 (1.191) / (5.820)
$c_{11}/3c_{12}$	14.535 / 16.503 (8.680) / (2.112)
C_{133}/C_{344}	−2.39 / −1.95 (−3.12) / (−1.10)
$C_{134}/-C_{444}$	0.82 / −0.33 (0.02) / (2.76)
$C_{114}/3C_{124}$	2.18 / 0.30 (−1.63) / (−0.45)
$C_{113}/C_{155}/3C_{144}/3C_{123}$	−1.93 / −1.39 / −2.07 / −1.23 (0.12) / (−2.00) / (−4.02) / (−8.82)
$C_{111}+5C_{112}/3C_{222}$	−13.14 / −20.25 (−19.35) / (−9.92)
$C_{111}+C_{112}/C_{113}+C_{222}$	−7.26 / −8.68 (−5.55) / (−3.20)

[a] Reference 30.
[b] Slash means equality on the left-hand side, but not necessarily on the right-hand side.

relations are not well satisfied in calcite, but the deviations are much less than for α-quartz. Judging from the fact that these deviations are not much different except for two cases ($C_{114}=3C_{124}$, $C_{111}+5C_{112}=3C_{222}$) from those in such ionic crystals as LiF and MgO [2–6] as well as NaCl,[25,26] the bond properties of calcite may be largely ionic.

If we assume that in the ionic-crystal Born-model approximation only the electrostatic and short-range repulsive terms are significant, then the difference between the observed C_{ijk} and the calculated $C_{ijk}{}^R$ for calcite can be attributed to the "electrostatic" contribution $C_{ijk}{}^e$. Since for all the carbonates the electrostatic interatomic potential $\phi^e(r_{\mu\nu})$ is the same for the corresponding ion pairs and the rhombohedral angle θ is approximately equal (Table IX), the corresponding lattice sums in Eq. (42) are identical for all the carbonates of the calcite type. (Here, we exclude the case of $NaNO_3$.) We can thus estimate the "electrostatic" contribution by only changing the lattice constants a, d and the unit cell volume V_c in Eq. (42), where $u_{ij}{}^R(r) \equiv D^3\phi_{ij}{}^R(r)$ is replaced by $u_{ij}{}^e(r)\equiv D^3\phi_{ij}{}^e(r)$. The results calculated in this manner are given in the first row of each crystal in Table XI. By adding the first row $C_{ijk}{}^e$ and the second row $C_{ijk}{}^R$ of each crystal, the total third-order constants C_{ijk} were semiempirically estimated in the third row. The variations of C_{111}, C_{222}, C_{333}, and C_{114} for the carbonate series are illustrated in Fig. 8, where the values calculated with another force law exponent $n_{12}=11$ for $CdCO_3$, $n_{12}=10$ for $MnCO_3$, $\frac{1}{2}(MgCa)CO_3$, $FeCO_3$, and $ZnCO_3$ are also plotted. It is noteworthy (Table XI and Fig. 8) that the variation of

negative C_{ijk} is very large (about 3 to 6 times), whereas that of positive C_{ijk} (C_{114}, C_{124}, C_{134}, C_{444}) is almost zero.

Lennard-Jones and Dent[67] have selected $n_{12}=11$ for $CdCO_3$ and $MnCO_3$ as a more favorable exponent, but could not assign an appropriate n_{12} to $FeCO_3$ and $ZnCO_3$. The higher-order elastic constant is a very convenient quantity, especially in examining the short-range, interatomic potential owing to its predominant contribution. If our exponents and force constants for $CaCO_3$ and $MgCO_3$ (Table IX) are correct, Fig. 8 seems to indicate that n_{12} is 10 for $CdCO_3$ and 11 for $MnCO_3$, $\frac{1}{2}(MgCa)CO_3$, $FeCO_3$, and $ZnCO_3$ in order to connect the points of the values C_{ijk} by smooth curves.

Perhaps the most useful result of the calculation of the repulsive contribution is that the experimental third-order constants (Table V) are confirmed as a reasonable set of values for calcite since the experimental and calculated values have the same relative magnitudes and signs (except C_{444}). To further analyze the experimental data, a detailed calculation including the electrostatic contribution is needed.

ACKNOWLEDGMENTS

The author wishes to express his sincere gratitude to Professor J. J. Gilman for introducing him to this field and for valuable and patient discussions of it. The author is also indebted to Professor A. V. Granato for the use of the apparatus involved in the hydrostatic pressure and temperature measurements. Thanks are also due to J. T. Holder for helpful discussions and the loan of part of his pulse-superposition method apparatus to T. C. Lloyd for assistance in constructing apparatus, to W. T. Stacy for reading the manuscript, and to Mrs. L. L. Hilton for her cheerful typing of it.

APPENDIX: GATE SHIFT OF THE GATED-CARRIER METHOD

Consider in the gated-carrier pulse-superposition method only the two echo trains out of many superposed-echo-trains which are all in phase with one another (Fig. 9). The upper figure (a) is the last applied (superposed) direct pulse and its echo-train and the lower (b) is the one applied a long time earlier whose echoes still do not vanish and are contributing to the interference condition. The number of cycles in one echo is reduced to five cycles for clarity instead of 10–20 cycles in the actual case. Under this initial interference condition the hatched cycles in echo A are exactly in phase with those in echo B. Now when the external conditions are changed and the sound velocity is increased, the echoes in (b) advance to the left [to the dotted envelopes of (b)] according to decrease in the transit time (the amount of this shift is different from echo to echo), and the hatched cycles in echo B are shifted to the open solid cycles in the dotted envelop. Echo B is no longer in phase with echo A in this situation. In order to keep the interference condition, the

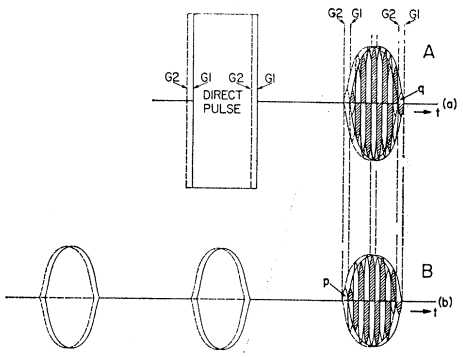

FIG. 9. Deviation from the exact interference condition due to gate shift in the gated-carrier pulse-superpositoin method.

carrier instead of repetition-rate frequency is changed (increased in this case) in the gated-carrier method. Then, when the carrier frequency is increased, the phase of echo A proceeds relative to the phase of echo B and the carrier cycles in echo A move to the open solid cycles, where the interference condition is again satisfied between the two echoes, A and B. However, if the gate position for echo A is kept at the same place, then not only the first half cycle p of echo B and the last half cycle q of echo A are left without interference, but also the interference between the open solid cycles enclosed by the solid envelop of echo A and those enclosed by the dotted envelop of echo B does not give rise to the same interference pattern as that in the previous interference condition. This is because each open solid cycle of echo A is different in size and shape from the corresponding hatched cycle of the same echo. That is, the different echo amplitude would be expected to appear in this new interference condition. If the gate position is slightly adjusted to the left, from G1 to G2 (higher repetition rate), exactly the same size and shape for each cycle of echo A can be obtained and the same interference pattern of the superposed echoes is produced again (the open dotted cycles of echo A).

In the actual practice the number of rf cycles, $f_n\tau$, for one round trip is about 100. If the velocity is increased by $10^{-4}(\Delta\tau=-10^{-4})$, then the change in the number of cycles is about 10^{-2} cycles for one round trip. In the pulse-superposition method, normally many echoes are superposed depending on the energy loss of the specimen, and in calcite even more than 20 echoes were observed for many modes used. If we assume that echo B in (b) is the 20th echo of this echo train, then the change in the number of cycles for 20 round trips, i.e., the shift of the echo due to this change of velocity is about 0.2 cycles. In this schematic figure this has been taken to be 0.5 cycles. If it is thought that not only one but many echoes are shifted from one another in this way in this method, though the degree of shift is different for all echoes, it is expected that this phenomenon might cause a large effect on the interference condition.

In fact, a sizable effect has been observed in measur-

ing the interference-carrier frequency when the repetition-rate frequency was adjusted. Also, when this adjustment was not made, high-frequency noise signals close to but a little off the repetition-rate frequency were observed being superposed upon the echo oscillation. This frequency was associated with this gate shift and could be calculated from the above idea.

In conclusion, this effect is attributed to the nonrectangular shape of echoes and the small number of cycles (10–20 cycles) involved in one echo.

PHYSICAL REVIEW VOLUME 172, NUMBER 3 15 AUGUST 1968

Ground State of Solid Neon

JEAN-PIERRE HANSEN*
Laboratoire de Physique Théorique et Hautes Energies,† Orsay, France
(Received 7 February 1968)

A variational calculation of the curve of ground-state energy versus density for solid neon is presented using a two-parameter wave function which takes correlations between pairs of atoms into account. A Monte Carlo method is used for the computation of the energy expectation value, the ground-state pressure, and the single-particle distribution function. The Lennard-Jones interatomic potential is assumed throughout, and various potential parameter values are discussed. If carefully determined experimental parameters are used, a pressure-versus-density curve is obtained which is in good agreement with experiment.

I. INTRODUCTION

AMONG the rare-gas crystals, solid helium and solid neon stand apart because of the important zero-point motion of their atoms. This is most marked for solid helium, which must be considered as a "quantum crystal" and has received considerable theoretical interest. Solid neon presents the same quantum character although to a lesser extent than solid helium, because the neon atomic mass is about five times larger than the He^4 atomic mass.

Throughout this paper as well as in most of the previous work it is assumed that the interaction between the rare-gas atoms can be described by the Lennard-Jones potential

$$v(r)=4\epsilon[(\sigma/r)^{12}-(\sigma/r)^{6}]. \quad (1)$$

The relative importance of quantum effects can be characterized by the value of the dimensionless parameter

$$\Lambda=\hbar/\sigma(m\epsilon)^{1/2},$$

where m is the mass of an atom in the lattice. For He^4, Λ is worth about 0.4, whereas for neon Λ equals about 0.08. Recently, Brown[1] has presented expressions for the ground-state energy and pressure of rare-gas solids including terms up to order Λ^2. Using these expressions and the experimental values of the sublimation energy and the lattice parameter of solid neon at 0°K, he determined the Lennard-Jones potential parameters ϵ and σ. The values obtained by Brown are given in Table I together with the values determined by second-virial coefficient measurements in the gas phase[2] and the values used by Bernardes[3] and by Nosanow and Shaw[4] in their calculations which will be discussed later. The three sets of values are seen to differ by a few percent. One of the purposes of this paper is to study the influence of these differences on the calculated ground-state properties.

Apart from Brown's lattice-dynamics approach including anharmonic terms, most other theoretical calculations of solid neon ground-state properties are variational. Bernardes,[3] as well as Nosanow and Shaw,[4] used a trial wave function which is a product of single-particle wave functions, each spherically symmetric around a lattice site. Nosanow and Shaw solved the Hartree equation for this problem and thus obtained the lowest possible ground-state energy in the single-particle approximation. Their results are given together with others in Table II. The fact that, using the same approximation, Bernardes obtained a lower energy with a one-parameter single-particle trial wave function can only be due to an error in his caclulations.

Table II clearly shows that there remains a 20 cal/mole difference between the Hartree ground-state energy and experimental results. In order to explain this difference Mullin[5] tried to take the correlations between atoms into account by using a Jastrow times

TABLE I. Lennard-Jones potential parameters.

	Brown[a]	2nd virial[b]	Bernardes[c]
σ(Å)	2.786	2.74	2.74
ϵ(°K)	36.76	35.6	36.2

[a] Reference 1.
[b] Reference 2.
[c] Reference 3.

* Present address: Laboratoire de Physique Théorique et Hautes Energies Bâtiment 211, Faculté des Sciences, 91-Orsay, France.
† Laboratoire associé au Centre National de la Recherche Scientifique.

[1] J. S. Brown, Proc. Phys. Soc. (London) **89**, 987 (1966).
[2] J. de Boer and A. Michels, Physica **5**, 945 (1938).
[3] N. Bernardes, Phys. Rev. **120**, 807 (1960).
[4] L. H. Nosanow and G. L. Shaw, Phys. Rev. **128**, 546 (1962).
[5] W. J. Mullin, Phys. Rev. **134**, A1250 (1964).